

1 **Terminal uridylyltransferases target RNA viruses as part of the innate**

2 **immune system in animals**

3

4 Jérémie Le Pen<sup>1,2,3,†</sup>, Hongbing Jiang<sup>4,#</sup>, Tomás Di Domenico<sup>1,3,5,#</sup>, Emma Kneuss<sup>1,6</sup>, Joanna  
5 Kosalka<sup>1,3</sup>, Christian Leung<sup>4</sup>, Marcos Morgan<sup>7,8</sup>, Christian Much<sup>7,8</sup>, Konrad L. M. Rudolph<sup>1,3,5</sup>,  
6 Anton J. Enright<sup>9</sup>, Dónal O’Carroll<sup>7,8</sup>, David Wang<sup>4</sup>, Eric A. Miska\*<sup>1,3,5</sup>

7 <sup>1</sup> Gurdon Institute, University of Cambridge, Tennis Court Road, Cambridge, CB2 1QN, United  
8 Kingdom

9 <sup>2</sup> Department of Biochemistry, University of Cambridge, 80 Tennis Court Road, Cambridge,  
10 CB2 1GA, United Kingdom

11 <sup>3</sup> Department of Genetics, University of Cambridge, Downing Street, Cambridge, CB2 3EH,  
12 United Kingdom

13 <sup>4</sup> Departments of Molecular Microbiology and Pathology & Immunology, Washington  
14 University in St. Louis School of Medicine, St. Louis, Missouri, United States of America

15 <sup>5</sup> Wellcome Trust Sanger Institute, Wellcome Trust Genome Campus, Cambridge, CB10 1SA,  
16 United Kingdom

17 <sup>6</sup> Cancer Research UK, Cambridge Institute, University of Cambridge, Cambridge, CB2 0RE,  
18 United Kingdom

19 <sup>7</sup> MRC Centre for Regenerative Medicine, Institute for Stem Cell Research, School of Biological  
20 Sciences, University of Edinburgh, 5 Little France Drive, Edinburgh, EH16 4UU, United  
21 Kingdom

22 <sup>8</sup> European Molecular Biology Laboratory (EMBL), Mouse Biology Unit, Via Ramarini 32,  
23 Monterotondo Scalo, 00015, Italy

24 <sup>9</sup> European Molecular Biology Laboratory (EMBL), European Bioinformatics Institute (EBI),  
25 Hinxton, Cambridge, CB10 1SD, United Kingdom

26 <sup>†</sup> Current address: Laboratory of Virology and Infectious Disease, The Rockefeller University,  
27 New York, New York, United States of America

28

29 # These authors contributed equally

30 \*Correspondence to: Eric A. Miska, email [eam29@cam.ac.uk](mailto:eam29@cam.ac.uk) phone +44-1223-767220

31

32 **RNA viruses are a major threat to animals and plants. RNA interference (RNAi) and the**  
33 **interferon response provide innate antiviral defense against RNA viruses. Here we**  
34 **performed a large-scale screen using *C. elegans* and its natural pathogen, the Orsay virus**  
35 **(OrV), and identified *cde-1* as important for antiviral defense. CDE-1 is a homologue of**  
36 **the mammalian TUT4/7 terminal uridylyltransferases; its catalytic activity is required for**  
37 **its antiviral function. CDE-1 uridylates the 3' end of the OrV RNA genome and promotes its**  
38 **degradation, independently of the RNAi pathway. Likewise, TUT4/7 uridylate influenza A**  
39 **virus (IAV) mRNAs in mammalian cells. Deletion of TUT4/7 leads to increased IAV mRNA**  
40 **and protein levels. We have defined 3' terminal uridylation of viral RNAs as a conserved**  
41 **antiviral defense mechanism.**

42

43 RNA viruses are a major threat to human health and food security. Understanding the fundamental  
44 mechanisms by which animals and plants combat viral infections might lead to new therapeutic  
45 antiviral approaches. RNA interference (RNAi) is an important antiviral pathway in most animals  
46 and plants: Dicer recognizes and cleaves the double-stranded viral RNA genome into virus-derived  
47 small interfering RNAs (viral siRNAs, viRNAs), which are loaded into Argonaute proteins to form  
48 the RNA-induced silencing complex (RISC) that in turn targets the viral RNA genome <sup>1</sup>.  
49 Vertebrates have additionally evolved a cellular signaling-based pathway, the interferon response  
50 (IR): upon recognition of foreign RNAs (i.e. double-stranded or bearing a 5' di/triphosphate),  
51 cytosolic receptors of the RIG-I family activate the IR which results in an antiviral state of the cell  
52 <sup>2,3</sup>. In the evolutionary arms race between viruses and their hosts, however, animals must have  
53 evolved a diverse range of antiviral strategies, to not solely rely on the RNAi or IR pathways.

54

55 Here, we develop a system for antiviral gene discovery using the nematode  
56 *Caenorhabditis elegans* (*C. elegans*) and identify 3' terminal uridylation of viral RNAs as a third  
57 antiviral mechanism in animals.

58

## 59 RESULTS

### 60 A forward genetic screen identifies new genes required for antiviral defense in *C. elegans*

61 We carried out a forward genetic screen to discover antiviral pathways in animals using *C. elegans*  
62 and its natural intestinal pathogen, the Orsay virus (OrV) <sup>4-12</sup>. OrV is a bipartite positive-strand  
63 RNA virus related to the *Nodaviridae* <sup>4</sup>. As is typical for positive sense RNA viruses, the genomic  
64 strand of the OrV is a template for translation. The OrV spreads horizontally in populations of *C.*  
65 *elegans*: it is taken up orally, infects only intestinal cells and probably exits through defecation <sup>4</sup>.  
66 While *C. elegans* lacks an interferon pathway, a RIG-I ortholog, DRH-1, acts in viral recognition.  
67 DRH-1 forms a Viral Recognition Complex (ViRC) with the *C. elegans* Dicer (DCR-1) and the  
68 RNA-binding protein RDE-4 to link viral recognition to a dedicated antiviral RNAi pathway,  
69 involving the Argonaute protein RDE-1 <sup>5,11,13,14</sup>. DRH-1 also induces a transcriptional immune  
70 response through a STAT-dependent signaling pathway (e.g. the gene *sdz-6*, as shown by qRT-  
71 PCR in Extended Data Fig. 1a) <sup>10,15,16</sup>. However, the antiviral function of the DRH-1-mediated  
72 stress response remains to be elucidated. *C. elegans* also elicits a “biotic stress response” upon  
73 OrV infection that is independent of DRH-1 and partially overlaps with transcriptional responses  
74 induced by other types of pathogens, possibly as a result of perturbations in cell homeostasis and/or  
75 mechanical integrity (e.g. the gene *lys-3*, encoding an antibacterial enzyme, as shown by qRT-PCR  
76 in Extended Data Fig. 1a) <sup>10</sup>. We generated a viral stress sensor transgene by placing the green  
77 fluorescent protein (GFP) under the control of the *lys-3* promoter (allele *mjIs228*; Fig. 1a). Upon

78 infection, the level of GFP expression in the intestine mirrored the viral load in wild type, *drh-1*  
79 and *rde-1* mutants (Extended Data Fig. 1b, c). We used chemical mutagenesis to screen ~50,000  
80 haploid genomes (Fig. 1b) and identified 16 isolates we named Ovid (Orsay Virus Immune  
81 Deficient; Fig. 1c and Supplementary Table 1). 13 out of 16 *ovid* mutants showed increased viral  
82 loads (Fig. 1c). *ovid-3,4,5,10,12* are compromised in somatic RNAi, as tested by RNAi knockdown  
83 of the gene *unc-22*, which normally results in impaired locomotion (Fig. 1c), and *ovid-3,4,10* carry  
84 new alleles of RNAi genes *mut-16*, *rde-4* and *rrf-1*, respectively (Table 1). To further stratify our  
85 Ovid isolates, we assayed DRH-1 pathway activation using the expression of the downstream  
86 induced gene *sdz-6* as readout (Fig. 1d). Only *ovid-1* phenocopied *drh-1* mutants and we  
87 subsequently demonstrated that *ovid-1* defines a new allele of *drh-1* (Fig. 1d). We identified a  
88 number of additional candidate genes (Table 1). *ovid-9* and *ovid-11* mutants are neither defective  
89 in canonical RNAi nor in the DRH-1 pathway and thus represent candidate genes for novel  
90 antiviral defense mechanisms.

91

## 92 **The terminal uridylyltransferase CDE-1 is required for antiviral defense in *C. elegans***

93 Whole-genome re-sequencing and genetic complementation tests revealed the causative mutation  
94 in *ovid-9* to be a single-nucleotide nonsense mutation in the *cde-1* gene (*mj414*, glutamine 910 to  
95 STOP) (Fig. 2a and Extended Data Fig. 2). *cde-1* encodes a catalytically active 3'-terminal RNA  
96 uridylyltransferase (TUT), which is a homologue of mammalian TUT4 and TUT7 enzymes<sup>15-17</sup>  
97 (Fig. 2b, c). The independently derived *cde-1* (*tm1021*) knockout strain also phenocopied viral  
98 stress sensor activation (Extended Data Fig. 3), high viral loads (Fig. 2d), and horizontal  
99 transmission of infection (Extended Data Fig. 3). RNA FISH revealed that viral infection is  
100 restricted to the intestine in *cde-1* and in *cde-1; drh-1* double mutants<sup>4,9</sup> (Extended Data Fig. 4a).

101 We validated that CDE-1 is present in the intestine using a GFP fusion <sup>16</sup> (Extended Data Fig. 4b).  
102 To disentangle between the functions of CDE-1 in different tissues, *cde-1* was exclusively  
103 expressed from an intestine-specific *vha-6p* promoter (Extended Data Fig. 4c). Animals with  
104 intestinal expression of *cde-1* became resistant to viral infection (Extended Data Fig. 4d), but kept  
105 a defect in meiotic chromosome segregation (Extended Data Fig. 4e), probably caused by CDE-1  
106 depletion in the germline <sup>15</sup>. CDE-1 contains a conserved triad of acid aspartic residues (DDD) in  
107 its nucleotidyltransferase domain. Mutation of the corresponding DDD triad to DAD (D1011A) in  
108 human TUT4 resulted in loss of catalytic activity <sup>18</sup>. A *cde-1* DAD mutant strain (Fig. 2a,c) showed  
109 similar viral susceptibility as the *cde-1* null mutants (Fig. 2d). In summary, we identify CDE-1-  
110 mediated 3' terminal uridylation as an antiviral activity in the intestine of *C. elegans*.

111

### 112 **CDE-1 exert its antiviral function independently of antiviral RNAi**

113 In eukaryotes, addition of 3' uridyl-tails (U-tails) by TUTs is a degradation signal that can engage:  
114 (i) the XRN-family of exoribonucleases for 5' to 3' RNA decay; (ii) the 3' to 5' exoribonuclease  
115 DIS3L2; (iii) the 3' to 5' exosome complex <sup>19-22</sup>. We sought to identify the RNA(s) targeted by  
116 CDE-1 in its antiviral role. CDE-1 is implicated in endogenous RNAi pathways that are restricted  
117 to the germline <sup>15</sup>. Small RNA sequencing on whole animals revealed that siRNAs are targeted by  
118 CDE-1 for 3' uridylation, miRNAs are occasionally targeted, and piRNAs are not targeted <sup>15</sup>  
119 (Extended Data Fig. 5a). The role of CDE-1 in small RNA function remains unclear as depletion  
120 of CDE-1 leads to only subtle changes in siRNA and miRNA steady state levels (Extended Data  
121 Fig. 5b, c). To understand if CDE-1 functions through modification of siRNAs in antiviral  
122 immunity, we tested *cde-1* mutants directly for defects in antiviral RNAi. During an antiviral RNAi  
123 response in *C. elegans*, the ViRC complex recognizes the dsRNA of the replicating viral genome

124 and dices it into sense and antisense ~23-nt long primary viRNAs, which are loaded into the RDE-  
125 1 Argonaute protein <sup>5</sup> (Fig. 3a). The RNAi response is further amplified by RNA-dependent RNA  
126 polymerase (RdRP, RRF-1) generated 22-nt long antisense secondary viRNAs, with a 5'  
127 triphosphate guanine (22G-RNAs), which are incorporated into secondary Argonaute proteins to  
128 silence viral amplification <sup>5</sup> (Fig. 3a). Thus, in an animal with functional antiviral RNAi, a high  
129 viral load should correlate with a high level of viRNAs. We measured primary and secondary  
130 viRNAs in different genetic backgrounds (Fig. 3b,c). All the mutants tested (*drh-1*, *rde-1*, *cde-1*)  
131 accumulate high levels of the virus as compared to wild type. In *drh-1* mutants, primary and  
132 secondary viRNAs are depleted when compared to wild type, despite the increase in viral load. In  
133 *rde-1* mutants, primary viRNAs are abundant but secondary viRNAs are depleted, as in *drh-1*. In  
134 contrast, *cde-1* mutants accumulate both primary and secondary viRNAs to a level that correlates  
135 with the high viral load. To determine if viRNAs can silence viral amplification in *cde-1* mutants,  
136 we carried out epistasis analysis using null mutants of *drh-1*, *rde-1* and *cde-1* (Fig. 3d,e). Both  
137 *cde-1;drh-1* and *cde-1;rde-1* double mutants showed an increase in viral load as compared to *drh-*  
138 *1* or *rde-1* on its own. We conclude that CDE-1 does not exert its immune function through the  
139 antiviral RNAi pathway.

140

### 141 **CDE-1 defines a novel antiviral immunity pathway**

142 In mammals, uridylation is coupled to poly(A) tail length where TUT4 and TUT7 preferentially  
143 uridylate mRNAs with short poly(A) tails (<25 nt) to facilitate their degradation <sup>23,24</sup> (Fig. 4a). We  
144 thus assessed the impact of CDE-1 on endogenous mRNA poly(A) tail lengths and terminal  
145 nucleotide addition in infected wild-type or *cde-1* mutant animals using TAIL-seq <sup>23,25</sup>. The *C.*  
146 *elegans* transcriptome revealed a bimodal distribution of poly(A) tail lengths, with a major peak

147 of poly(A) tails of ~40 nt, and a second peak of poly(A) tails of ~10 nt (Fig. 4b; using our method  
148 we could not assess transcripts with poly(A) tails > 79 nt). In *cde-1* mutants, there is a shift of the  
149 major ~40 nt peak to ~36 nt and an increase in transcripts with shorter poly(A) (Fig. 4b). We infer  
150 that CDE-1 promotes the degradation of transcripts with short poly(A) tails in *C. elegans* too.  
151 However, CDE-1 had no global effect on the poly(A) tail distribution of OrV-induced stress  
152 response genes (Extended Data Fig. 6a). Also, the OrV-induced stress response was stronger in  
153 *cde-1* mutants than in wild-type upon infection (Extended Data Fig. 6b), reflecting the difference  
154 in viral load between these two strains. This indicates that CDE-1 is not required for the OrV-  
155 induced stress response. Although we cannot formally rule out that CDE-1 may regulate an  
156 endogenous target(s), the evidence indicates this is not CDE-1's principal function in antiviral  
157 immunity.

158  
159 Instead, we postulated that the viral RNA genome itself may be uridylated by CDE-1. U-tails can  
160 only be observed on a small percentage of cellular RNAs as uridylated RNAs are prone to be  
161 degraded<sup>24</sup>. To detect uridylated Orsay RNA degradation intermediates, we carried out 3' rapid  
162 amplification of cDNA ends (RACE) followed by high-throughput sequencing of the OrV RNAs  
163 extracted from *C. elegans* two days postinfection (RACE-seq; Extended Data Fig. 7a). Mono(U)  
164 tails constituted the most abundant fraction of non-templated nucleotides detected at the 3' end of  
165 both OrV RNA1 and OrV RNA2 (Fig. 4c-e). For both RNA1 and 2, U-tailing was lost in two  
166 independent *cde-1* mutant alleles. In contrast, *drh-1* and *rde-1* mutants showed similar levels of  
167 viral RNA U-tails to wild-type, indicating that U-tailing is independent of viral load and that CDE-  
168 1 is not in limited quantities (Extended Data Fig. 7b,c). OrV RNA1 and RNA2 have a terminal  
169 uridylyl residue in their genome such that the addition of an extra non-templated uridine by CDE-

170 1 forms a UU termination (Fig. 4d), which is a signal for uridylation-dependent RNA decay<sup>19,21</sup>.  
171 The two XRN paralogs in *C. elegans* (XRN-1 and XRN-2) and the exosome components (e.g.  
172 DIS-3, EXOS-2) are essential<sup>26,27</sup>, and these RNA degradation pathways normally act redundantly  
173 on uridylated RNAs<sup>24</sup>. We therefore subjected *C. elegans* to a short (24 hours) RNAi treatment to  
174 effect a partial knockdown of *cde-1*, the exonuclease *disl-2* (the *C. elegans* DIS3L2 homologue),  
175 the exosome components *exos-2* and *dis-3*, and the exonuclease *xrn-2*. Treated animals, which  
176 appeared superficially wild type, were infected with OrV for 24 hours. The frequency of U-tails in  
177 OrV RNA2 was measured by RACE-seq (Fig. 4f). ~4% of OrV RNA2 were uridylated in animals  
178 exposed to the empty vector control RNAi, compared to ~1% in *cde-1* knockdown. RNAi  
179 treatments against *disl-2* did not affect the U-tail frequency. We measured a 1.4 to 1.7 fold increase  
180 in U-tail frequency upon RNAi treatment against *exos-2*, *dis-3* and *xrn-2*, suggesting that these  
181 factors each contribute to the degradation of uridylated viral RNAs, in accordance with a study  
182 that shows that DIS3 and the exosome can degrade viral RNAs in *Drosophila* and human cells<sup>28</sup>.  
183 We conclude that *C. elegans* uses uridylation of the OrV as an innate immune defense. This  
184 mechanism acts in parallel to antiviral RNAi to combat viral infection (Fig. 5).

185

### 186 **Terminal uridylyltransferases target viral RNAs in mammalian cells**

187 The U-tail modification is conserved in eukaryotes and could impact a broad range of viruses in a  
188 variety of hosts<sup>29</sup>. We tested if U-tailing affects the replication of Influenza A virus (IAV), which  
189 can infect human and murine cells. The IAV genome consists of eight antisense RNA segments  
190 (viral RNAs, vRNAs) from which the viral RdRP produces: (i) the sense complementary RNAs  
191 (cRNAs), which serve as templates to produce more vRNAs; and (ii) the mRNAs that are 3'  
192 polyadenylated and exported to the cytosol for translation into viral proteins<sup>30</sup> (Fig. 6a). We



193 examined the 3' end of a set of IAV RNAs, at 8 hours post-infection (hpi), in A549 human lung  
194 cells by RACE-seq. We could not detect U-tails at the ends of vRNAs or cRNAs. In contrast, viral  
195 mRNAs were highly uridylated at their 3' end, with ~77% of the IAV Nucleoprotein (NP) mRNA  
196 containing a U-tail, and a di(U)-tail being the most common type of 3' end (~32%) (Fig. 6b-e).  
197 The IAV NP mRNA is also uridylated (~40-50%) at 8 hpi in mouse embryonic fibroblasts (MEFs),  
198 but uridylation was lost in MEFs deficient in both *Tut4* and *Tut7*<sup>23</sup> (Fig. 6f). Thus TUT4/7 can  
199 uridylate the 3' end of viral RNAs in mammalian cells. The RACE-seq can only detect IAV  
200 mRNAs with poly(A) tails of <70 nt; it is possible that some IAV mRNAs with very long poly(A)  
201 tails are less prone to be uridylated. To test the impact of TUT4/7 on IAV, we measured the  
202 quantity of NP mRNA by qRT-PCR in infected MEFs (Extended Data Fig. 8a). The IAV NP  
203 mRNA accumulated more rapidly and to a higher level at the peak in MEFs *Tut4/7* KO cells (peak  
204 at 8 hpi) compared to WT cells (peak at 16 hpi) before decreasing later in infection (24 hpi).  
205 Consistent with the difference in mRNA levels, the NP mRNA-encoded viral nucleoprotein (NP)  
206 accumulated more rapidly in MEFs *Tut4/7* KO cells compared to WT during the first eight hours  
207 of infection (Extended Data Fig. 8b). Accordingly, more infected cells overall were observed in  
208 MEFs *Tut4/7* KO compared to WT (Fig. 6g). In conclusion, TUT4/7 could act as an early barrier  
209 against IAV infection in mammalian cells. Although we cannot rule out that TUT4/7 may impact  
210 other steps of the IAV viral cycle, such as entry, our data strongly supports a model where TUT4/7  
211 act by reducing the expression levels of IAV mRNAs during the early stages of IAV infection in  
212 MEFs, leading to a decrease in viral protein levels and rates of infection. Future studies will need  
213 to address the antiviral function of TUT4/7 in a variety of relevant host-virus models.

214

215

## 216 **DISCUSSION**

217 Previously, we have shown that the antiviral RNAi pathway and DRH-1 are central to the innate  
218 immune response of *C. elegans*<sup>5</sup>. Here, we demonstrate that the terminal uridylyltransferases also  
219 play a critical role in antiviral immunity, uridylylating viral RNAs (with 1-2 Us) to mark them for  
220 degradation. It is unclear how terminal uridylyltransferase recognize viral RNAs as *bona fide*  
221 targets. Receptors of the RIG-I family commonly recognize pathogen-associated patterns at the 5'  
222 termini of viral RNAs. In contrast, terminal uridylyltransferases interact with the 3' termini of  
223 cytosolic RNAs with no poly(A)-tail or a short poly(A)-tail. As many RNA viruses, like OrV, lack  
224 a poly(A) tail at the 3' termini of their RNA genomes, this may be a pathogen-associated pattern-  
225 recognition feature. We speculate that the IAV mRNAs and a fraction of the OrV RNAs are  
226 vulnerable to TUTs when exposed in the cytosol for translation. In conclusion, we find that  
227 terminal uridylyltransferases are potent antiviral factors during the early stages of RNA virus  
228 infections in *C. elegans* and in mammalian cells. This finding supports a scenario where eukaryotic  
229 mRNA decay pathways originally evolved as intrinsic cellular defenses against pathogens<sup>31,32</sup>.  
230 Vertebrates also benefit from the interferon response and adaptive immune system, serving as  
231 potent lines of defense against pathogenic viruses; future studies will thus need to address the  
232 relative importance of antiviral uridylation in whole organisms. Terminal uridylyltransferases are  
233 widely conserved in eukaryotes and could potentially target a wide range of RNA viruses<sup>29</sup>.  
234 Perhaps as a response to this threat, some viruses evolved to protect their RNA termini, such as  
235 single-stranded RNA viruses of the *Flaviviridae* family, which have highly structured 3' ends  
236 resistant to degradation by cellular exonucleases<sup>33</sup>. Our study illustrates that the 3' termini of viral  
237 RNAs are key in the evolutionary arms race between viruses and their hosts.

238

## 239 **METHODS**

### 240 **Genetics**

241 Animals were grown on agar plates, at 20°C, and fed with *E. coli* strain HB101 (obtained from the  
242 *Caenorhabditis* Genetics Center, University of Minnesota, USA). Standard *C. elegans* procedures  
243 were used for maintenance and genetic crosses<sup>34</sup>. The wild-type strain refers to Bristol N2 unless  
244 stated otherwise. All strains used in this study are listed in the Supplementary Table 2.

245

### 246 **PCR primers**

247 All PCR primers used in this study are listed in the Supplementary Table 3.

248

### 249 **Viral filtrate preparation**

250 Viral filtrate was prepared as in<sup>8</sup>. Briefly, JU1580 animals were first stably infected by the Orsay  
251 virus (OrV) in solid culture and then transferred in a liquid culture containing OP50 bacteria for  
252 seven days. The liquid culture with infected JU1580 was then centrifuged at 16,000 g for 30 min  
253 and the supernatant was filtered (0.22 µm filter) to produce the viral filtrate (stored at -80°C).

254

### 255 **Transgenesis of *C. elegans* with the *lys-3p::GFP* viral stress sensor**

256 The 452 bp region upstream of the *lys-3* start codon and the first 57 bp of the coding region of *lys-*  
257 *3* were used as a promoter and cloned into an entry clone using Multi-Site Gateway cloning  
258 (Invitrogen) according to manufacturer's instructions. The *lys-3* donor plasmid was validated by  
259 sequencing. Gateway technology was then used to clone the *lys-3* fragment in frame with a GFP  
260 cDNA. The 3' UTR of the *tbb-2* (tubulin, beta) gene was used. The *lys-3p::GFP:tbb-2-3'UTR*  
261 plasmid was amplified and purified according to Invitrogen's instruction. The *C. elegans*

262 microinjection mix was: 5 ng/μl plasmid *lys-3p::GFP:tbb-2-3'UTR*; 5 ng/μl co-injection marker  
263 (*myo-2::mcherry::unc-54-3'UTR*, pharynx expression) and 85 ng/μl 1 kb Invitrogen ladder in 1×  
264 injection buffer (20 mM potassium phosphate, 3 mM potassium citrate, pH 7.5). This mix was  
265 microinjected into the gonads of *rde-1 (ne219)* mutants to generate a multicopy extrachromosomal  
266 array (allele *mjEx547*). X-ray integration of the transgene into the *C. elegans* genome was  
267 performed as described previously<sup>35</sup>. Animals carrying an integrated transgene (allele *mjIs228*)  
268 were outcrossed three times to generate SX2635 (lacking *ne219*), referred to as wild-type viral  
269 stress sensor strain in this study.

270

#### 271 **Confocal images of the biostress reporter**

272 A 2% agar pad was used on top of a glass slide and a drop of 10 μM tetramisol in M9 medium was  
273 placed on this agar pad. Animals were picked into the tetramisol solution. Imaging was performed  
274 with an Olympus Upright FV1000 microscope at 10× or 20× magnification, as specified, using the  
275 FluoView image software (Olympus). Identical microscope settings were used for all images  
276 within a figure.

277

#### 278 **Forward genetic screen for Ovid screen isolates**

279 Approximately 4,000 viral stress sensor transgenic animals were mutagenized using ethyl  
280 methanesulfonate (EMS) as described in<sup>34</sup> and<sup>36</sup>. Approximately 50,000 F2 animals were infected  
281 for 3-4 days and ~2,000 animals showing intestinal GFP were picked individually for re-testing.  
282 16 F2 families showed transmission of the viral stress sensor activation. Bleach treatment  
283 confirmed that removing OrV lead to a loss of intestinal GFP signal.

284

285 ***C. elegans* infection by the Orsay virus**

286 Animals were either infected for four days as asynchronous populations or for two days as  
287 synchronous populations. Infections of asynchronous populations were performed as in <sup>5</sup>. Briefly,  
288 two L4 hermaphrodites were distributed in each 50 mm plates and, on the next day, 20 µl of viral  
289 filtrate was spread on the plates. Animals were harvested (for viral load measurement) or observed  
290 under a Leica M165 FC fluorescent microscope (for scoring of the viral stress sensor) four days  
291 post-infection (4 dpi). This method was typically used for the characterization of the Ovid screen  
292 isolates. For the infection of synchronous populations, 200 animals at the larval stage L1 were  
293 deposited on each 50 mm plate. On the next day, L2 animals were infected with 20 µl of viral  
294 filtrate homogeneously spread on the plate. Plates were kept up-side-up for 24 hrs. Animals were  
295 harvested for viral load measurement at 2 dpi. This method was used to measure the viral load in  
296 *cde-1* mutants, as indicated in the figure legends.

297

298 **RNA level measurement by qRT-PCR**

299 Harvested animals were washed three times by pelleting-resuspension in M9 solution. Lysis and  
300 qRT-PCR was then performed from 5 µl of animal pellet using the Power SYBR Green Cells-to-  
301 Ct kit (Ambion, Austin, TX) as described in <sup>5</sup>. The primers M1835 and M1836 <sup>13</sup>, and M4410 and  
302 M4411 <sup>4</sup>, were used to measure RNA levels of *gapdh* and OrV gRNA1, respectively.

303

304 **RNAi-mediated knockdown of *unc-22***

305 All the bacterial feeding clones used in this study were a kind gift from the laboratory of Julie  
306 Ahringer. Bacteria were grown in LB-Ampicillin (50 µg/ml) for 6 hrs, then seeded onto 50 mm  
307 NGM agar plates containing 1 mM IPTG and 25 µg/ml Carbenicillin at a volume of 300 µl bacterial

308 culture per plate and left to dry at room temperature, protected from the light, for 48 hrs. Two L4  
309 animals were picked onto each RNAi plates and the young adult progeny were scored for the  
310 phenotype of interest after five days.

311

### 312 **Transgenesis of *C. elegans* with the CDE-1::GFP fosmid and imaging**

313 The modified fosmid WRM064A\_D06 where the GFP sequence is added at the N-terminal end of  
314 *cde-1* was provided by the TransgeneOme Project (Max Planck Institute of Molecular Cell Biology  
315 and Genetics, TransgeneOme Unit, Pfothenhauerstr. 108, 01307 Dresden, Germany; construct  
316 09318202437763223 H08)<sup>37</sup>. The construct was injected into the gonad of N2 animals to produce  
317 an extrachromosomal array (as described for the biostress reporter), using a *myo-3p::mCherry::unc-54-3'UTR*  
318 construct as a co-injection reporter. Transgenic animals (strain SX3123; allele *mjEx594*) were imaged with an Olympus Upright FV1000 microscope at 10x  
319 magnification.  
320

321

### 322 **Fluorescence in situ hybridization of the Orsay virus RNA2**

323 Animals were harvested in 15 ml of nanopure water and washed three times by pelleting-  
324 resuspension in nanopure water. Animals were then transferred to 1.5 ml tubes with a glass pipette.  
325 1 ml of fixative solution (4% formaldehyde in 1X PBS) was added and samples were incubating  
326 at room temperature, on a rotating wheel, for 45 min. Nematodes were then washed twice by  
327 pelleting-resuspension in 1 ml of 1x PBS. Pellet of animals was resuspended in 1 ml 70% ethanol  
328 and stored at 4°C. After removal of the ethanol, fixed nematodes were washed once in 1 ml of  
329 wash solution (10% formamide, 2X SSC). The animal pellet was resuspended in 100 µl of  
330 hybridization solution (10% dextran sulfate, 2X SSC, 10% formamide) with 1 µl 1:50 of the probe

331 v1580-RNA2-TexRed (ACCATGCGAGCATTCTGAACGTCA), a kind gift of Marie-Anne  
332 Félix, and incubated overnight at 30°C protected from the light. The next day, animals were  
333 washed three times in wash solution by pelleting-resuspension. Eventually, animals were  
334 resuspended in 1 ml wash solution with DAPI and incubated at 30°C for 30 min. Samples were  
335 centrifuged and supernatant was discarded. The animal pellet was resuspended in 1 ml of 2X SSC  
336 solution and stored at 4°C protected from light. Animals were then placed on a glass slide, in a  
337 drop of Vectashield anti-fade solution (Vector). Imaging was performed on an Olympus Upright  
338 FV1000 at 40x magnification, using the FluoView image software (Olympus). Same settings of  
339 fluorescence were used for all images compared.

#### 340 **Transgenesis of *C. elegans* with the *vha-6p::gfp* plasmid and viral load measurement**

341 The 878 bp region upstream of the *vha-6* start codon was used as a promoter and cloned into an  
342 entry clone using Multi-Site Gateway cloning (Invitrogen) according to manufacturer's  
343 instructions. The *vha-6p* donor plasmid was validated by sequencing. Gateway technology was  
344 then used to clone the *vha-6p* upstream of (i) the GFP cDNA, or (ii) the full length *cde-1* gene  
345 (from ATG to STOP with endogenous introns). The 3' UTR of the *tbb-2* (tubulin, beta) gene was  
346 used. The *vha-6p::GFP::tbb-2-3'UTR* and *vha-6p::cde-1::tbb-2-3'UTR* plasmids were amplified  
347 and purified according to Invitrogen's instruction. The *C. elegans* microinjection mix was: 10 ng/μl  
348 plasmid *vha-6p::GFP::tbb-2-3'UTR*; 10 ng/μl plasmid *vha-6p::cde-1::tbb-2-3'UTR*; 5 ng/μl co-  
349 injection marker (*myo-2::mcherry::unc-54-3'UTR*, pharynx expression) and 75 ng/μl 1 kb  
350 Invitrogen ladder in 1× injection buffer (20 mM potassium phosphate, 3 mM potassium citrate, pH  
351 7.5). This mix was microinjected into the gonads of *cde-1* (*tm1021*) mutants to generate a  
352 multicopy extrachromosomal array (allele *mjEx595*). *vha-6p* driven GFP expression was only  
353 observed in the intestine. 100 animals carrying the extrachromosomal array were manually

354 selected for infection (from the L2 larval stage to young adult).

355

### 356 **Small RNA sequencing**

357 Small RNA libraries were prepared from infected animals as previously described in <sup>5</sup>. We used  
358 pellets of animals, washed three times in M9 solution and resuspended in 1 ml of TriSure (Bioline)  
359 as a starting material. RNA extraction was performed according to manufacturer's instructions.  
360 Some populations of siRNAs (including secondary viRNAs) contain a characteristic 5'  
361 triphosphate group that has to be replaced by a 5' monophosphate to allow the 5' ligation step of  
362 the library preparation. For this purpose, 1 µg of RNA was put in solution with 1X 5'p  
363 polyphosphatase buffer and 1 µl of 5' polyphosphatase (Epicentre) for a total volume of 20 µl,  
364 incubated for 30 min at 37°C and then submitted to phenol purification and resuspended in 5 µl of  
365 nuclease-free water. Treated RNA sample was entirely used as starting material for the TruSeq  
366 Small RNA kit (Illumina), following the manufacturer's instructions, to make the so-called 5'  
367 independent libraries. So-called 5' dependent libraries were made by a similar procedure but  
368 without polyphosphatase treatment, so that only 5' monophosphate siRNAs (such as primary  
369 viRNAs) could be cloned. Libraries were submitted to the Gurdon Institute sequencing facility for  
370 Illumina HiSeq sequencing (SR36). Small RNA sequencing data was aligned to the Ensemble  
371 WBcel235 release of the *C. elegans* genome using STAR <sup>38</sup> (v2.5.1b). Briefly, the aligner will  
372 allow untemplated residues at the ends of an aligned sequence when run in local mode.  
373 Untemplated 3' sequences were extracted and analysed using custom Python scripts. Details of the  
374 analyses for each small RNA subtype can be found in the source code. For miRNA differential  
375 expression, reads were counted against the miRBase miRNA annotations (miRBase21 hairpins,



376 WBcel235 genome) using featureCounts<sup>39</sup> (v1.5.0-p1). Differential expression analysis was  
377 performed on the counts using DESeq2<sup>40</sup> (v1.10.1).

378

### 379 **CRISPR/Cas9 for *cde-1* catalytic dead mutant**

380 A CRISPR/Cas9-mediated mutation of *cde-1* was generated as previously described<sup>41</sup>. Guide  
381 RNA: UUUGCUGUCAAAUCCUUUGG. Homologous recombination template:  
382 TCAGCTATTGCTATTTGTTTGAGATTCGGAGATGGAGATGTTCCGCCTAAAGACTTG  
383 ACAGCAAAAGAAGTTATTCAGAAAAGTGAATCCGTTCTCAGAAAATGTCATTT. Only  
384 the D1069A missense mutation was introduced, as verified by sequencing.

385

### 386 **TAIL-seq**

387 The TAIL-seq was performed as previously described in<sup>25</sup>. Tail-seq libraries were processed using  
388 Tailseeker 2<sup>25</sup>. The 5' and 3' libraries were subsequently adapter trimmed using cutadapt 1.10<sup>42</sup>  
389 with Illumina small RNA-seq adapters and filtered to a minimum length of 5bp. Trimmed 5' reads  
390 were mapped with STAR 2.5.2a<sup>38</sup> against a combined meta-genome consisting of the *C. elegans*  
391 reference genome WBcel235<sup>43</sup> and the OrV genome<sup>4</sup>. Mapping was performed in end-to-end  
392 mode allowing no mismatches and a gap opening and extension penalty of 10,000. Reads were  
393 assigned to genes with bedtools 2.26.0<sup>44</sup>. Subsequently, 3' reads without poly(A) tail or too many  
394 dark cycles were removed from the data. For the subsequent analysis, all *C. elegans* tags with  
395 poly(A) tail length equal to zero were discarded. Average poly(A) tail lengths and uridylation  
396 lengths for each sample were calculated as the arithmetic mean weighted by the support for each  
397 tag, reported by Tailseeker 2. The complete code is at <https://github.com/klmr/poly->  
398 [u/tree/submitted](https://github.com/klmr/poly-).

399

400 **mRNA libraries for deep sequencing**

401 mRNA libraries were prepared from three biological replicates per sample, using the NEBNext  
402 Ultra RNA non-directional Library kit with poly(A) selection (NEB), according to manufacturer's  
403 instructions. Libraries were submitted to the Gurdon Institute sequencing facility for Illumina  
404 HiSeq sequencing (SR30). Differentially expressed genes were then called using EdgeR<sup>45</sup>.

405

406 **3' RACE-seq on the Orsay virus RNAs**

407 The 3' RACE was performed on the same RNA input than that used for small RNA libraries,  
408 without polyphosphatase treatment. 200 ng of RNA were submitted to 3' ligation using the TruSeq  
409 Small RNA kit (Illumina), following the manufacturer's instructions. 3' ligated RNA was used for  
410 reverse-transcription, still using the TruSeq Small RNA kit whilst bypassing the 5' ligation step.  
411 The 3' end of OrV RNA1 (or RNA2) genome was amplified by PCR ("PCR1") from 2 µl of cDNA,  
412 using the primers M7454 and M7456 (or M7455 and M7456) and the Phusion High-Fidelity Taq  
413 Polymerase (NEB) with CG buffer, according to manufacturer's instructions. The thermocycler was  
414 programmed to 30 seconds at 98°C; 15 cycles of 5 seconds at 98 °C followed by 20 seconds at  
415 60°C and 10 seconds at 72°C. The 5' adapter sequence from the TruSeq Small RNA kit was then  
416 introduced at the 5' end of the amplicons by PCR ("PCR2") using the primers M7456 and M7601  
417 for OrV RNA1 (or M7456 and M7602 for the OrV RNA2), using 2 µl of 1/10 diluted amplicon  
418 from PCR1 as a template and the same PCR conditions than that used in PCR1. The amplicons  
419 from PCR2 were purified using the DNA Clean & Concentrator-5 kit (Zymo Research) and  
420 resuspended in 10 µl of water. Resulting DNA was used as an input for the PCR amplification step  
421 of the TruSeq Small RNA kit, following the manufacturer's instructions. Libraries were submitted

422 to the Gurdon Institute sequencing facility for Illumina HiSeq sequencing (PE100). The libraries  
423 were run on a 10% polyacrylamide gel for size selection (the amplicons could be visualized under  
424 UV light and the bands were cut at the same distance of migration for all samples). Paired-end  
425 reads obtained from the 3' RACE experiment on the viral genome show overlap. The PEAR  
426 software <sup>46</sup> was used to merge the paired reads into a single read (v0.9.6, default parameters).  
427 Merged reads not starting with the targeted 3' viral genome sequence fragment were discarded.  
428 The targeted viral genome sequence was removed from the remaining reads using custom python  
429 scripts ([https://github.com/tdido/cde-1\\_analysis](https://github.com/tdido/cde-1_analysis)). The resulting sequences representing the  
430 untemplated tails were analyzed using custom python scripts.

431

#### 432 **RNAi-mediated knockdown of *exonucleases***

433 Synchronized animals were grown on normal HB101 food until the L2 larval stage and then  
434 transferred RNAi food. Animals were left on RNAi plate (24 hours prior to infection) and infected  
435 for 24 hours, from the old L3/young L4 larval stages to adult. RACEseq was performed as  
436 described above.

437

#### 438 **Cell culture**

439 MEF cells were cultured with DMEM (GIBECO) supplemented with 12.5% FBS, 2mM L-  
440 glutamine, non-essential amino acid, 100 units/ml penicillin/streptomycin, 100 uM  $\beta$ -  
441 mercaptoethanol (Sigma). Cells were splitted 1:4 and passaged every three days. A549 cells were  
442 cultured with DMEM (GIBECO) supplemented with 10% FBS, 2mM L-glutamine, non-essential  
443 amino acid, 100 units/ml penicillin/streptomycin and 25mM HEPES.

444

445 **Generation of *Tut4/7* CTR and KO MEFs**

446 *Tut4/7* CTR and KO MEFs were derived from E13.5 embryos from crosses  
447 of *Tut4<sup>+/fl</sup>;Tut7<sup>+/fl</sup>;R26<sup>+/+</sup>* and *Tut4<sup>+/fl</sup>;Tut7<sup>+/fl</sup>;R26<sup>ERT-cre/ERT-cre</sup>* mice by standard procedures and  
448 immortalized at passage 2 by two consecutive infections with pBabeSV40LT. Cre-mediated  
449 deletion to obtain *Tut4/7* null alleles was induced with 600 nM 4-hydroxytamoxifen for three days  
450 <sup>23</sup>.

451

452 **A549 and MEF cells infection by Influenza A virus and RACE-seq**

453 Influenza A virus (A/WSN/1933, H1N1) used in this study was titrated on MDCK cells. All the  
454 inoculation MOI of influenza A virus described here and below was calculated as an equivalent  
455 MOI on the originally titrated MDCK cells.

456 A549 or MEF cells were trypsinized and seeded as  $2 \times 10^6$  cells per T25 flask one day before  
457 infection. 16 hours after seeding, culture media were removed and cells were washed once with  
458 pre-warmed DMEM. Influenza A virus (A/WSN/1933, H1N1) were inoculated at MOI 3 diluted  
459 with 1000  $\mu$ l DMEM supplemented with 0.1% BSA (D0.1B). Cells were trypsinized and collected  
460 8 hours post infection. 750  $\mu$ l TRIzol were added into each infected sample and were then freezed  
461 at -80 °C. RNA extraction was performed according to the standard TRIzol procedure.

462 For the A549 RACE-seq, 2  $\mu$ g of RNA were submitted to 3' ligation using the TruSeq Small RNA  
463 kit (Illumina), following the manufacturer's instructions. 3' ligated RNA was used for reverse-  
464 transcription, still using the TruSeq Small RNA kit (except that the Invitrogen Superscript III was  
465 used instead of the Superscript II) whilst bypassing the 5' ligation step. The RT final volume was  
466 12.5  $\mu$ l. After the RT, water was added to the samples to reach 18.5  $\mu$ l, final volume. The 3' end  
467 of IAV RNAs were amplified by PCR ("PCR1") from 2  $\mu$ l of cDNA, using the left primers M8443,

468 M8444, M8451, M8452, M8453, M8454, M8455, M8456 (depending on the target, see the  
469 Supplementary Table 3) with the right primer M7456 and the NEB Q5 polymerase, according to  
470 manufacturer's instructions (25  $\mu$ l reaction). The thermocycler was programmed to 30 seconds at  
471 98°C; 5 cycles of 5 seconds at 98 °C followed by 20 seconds at 60°C and 20 seconds at 72°C.  
472 Each PCR product was purified using the DNA Clean & Concentrator-5 kit (Zymo Research) and  
473 eluted in 11  $\mu$ l of water. The 5' adapter sequence from the TruSeq Small RNA kit was then  
474 introduced at the 5' end of the amplicons by PCR ("PCR2") using the left primers M8459, M8460,  
475 M8467, M8468, M8469, M8470, M8471, M8472 (depending on the target, see the Supplementary  
476 Table 3) with the right primer M7601, using 10  $\mu$ l of purified PCR1 amplicon as a template and  
477 the same PCR conditions that used in PCR1. Again, the amplicons from PCR2 were purified using  
478 the Zymo columns and eluted in 11  $\mu$ l of water. Resulting DNA was used as an input for the PCR  
479 amplification step of the TruSeq Small RNA kit, following the manufacturer's instructions.  
480 Libraries were submitted to the Gurdon Institute sequencing facility for Illumina HiSeq sequencing  
481 (PE100). The libraries were run on a 10% polyacrylamide gel for size selection (the amplicons  
482 could be visualized under UV light and the bands were cut at the same distance of migration for  
483 all samples). Paired-end reads obtained from the 3' RACE experiment on the viral genome show  
484 overlap. The PEAR software <sup>46</sup> was used to merge the paired reads into a single read (v0.9.6,  
485 default parameters). Merged reads not starting with the targeted 3' viral RNA sequence fragment  
486 were discarded. The targeted viral genome sequence was removed from the remaining reads using  
487 custom python scripts ([https://github.com/tdido/cde-1\\_analysis](https://github.com/tdido/cde-1_analysis)). The resulting sequences  
488 representing the untemplated tails were analyzed using custom python scripts. The MEFs RACE-  
489 seq was identical to the A549 cells RACE-seq, except: (i) the starting material was 1  $\mu$ g, (ii) the  
490 Invitrogen Superscript II was used for the RT, (iii) PCR1 and PCR2 had 10 cycles each.

491

492 **MEFs infection by Influenza A virus and qRT-PCR**

493 MEF cells were trypsinized and seeded as  $8 \times 10^4$  cells per well of 24-well plate one day before  
494 infection. 16 hours after seeding, culture media were removed and cells were washed once with  
495 pre-warmed DMEM. Influenza A virus (A/WSN/1933, H1N1) were inoculated at MOI 3 diluted  
496 with 250  $\mu$ l DMEM supplemented with 0.1% BSA (D0.1B). Cells were trypsinized and collected  
497 8, 16 and 24 hours post infection. 350  $\mu$ l TRIzol were added into each infected sample. RNA was  
498 extracted using Direct-zol™ RNA MiniPrep (Zymo Research) purification according to the  
499 manufacture's protocol and was finally eluted into 60  $\mu$ l RNase/DNase free water. The extracted  
500 RNA was subjected to strand specific qRT-PCR to quantify influenza virus replication as described  
501 in <sup>47</sup>.

502

503 **MEFs infection by Influenza A virus and FACS assay**

504 MEF cells were trypsinized and seeded as  $1 \times 10^4$  cells per well of 96-well plate one day before  
505 infection. 16 hours after seeding, culture media were removed and cells were washed once with  
506 pre-warmed DMEM. Influenza A virus (A/WSN/1933, H1N1) were inoculated at MOI 3 diluted  
507 with 50  $\mu$ l DMEM supplemented with 0.1% BSA (D0.1B). Inoculum was removed after 1 hour  
508 of incubation at 37 °C. The infected cells were cultured with MEF cell culture medium with  
509 2.5% FBS. 8 hours post inoculation, culture media were removed and cells were trypsinized  
510 through incubation with 30  $\mu$ l 0.05% trypsin for 3 minutes at 37 °C. Trypsinized cells were  
511 resuspended with 70  $\mu$ l of P2F (PBS with 2% FBS) and then fixed with 100  $\mu$ l 4% PFA for 15  
512 minutes. Fixed cells were centrifuged at 300g for 5 minutes and then washed once with 100  $\mu$ l  
513 P2F. Cells were then permeablized with buffer (0.1% Saponin, 10mM HEPES, 0.025% Sodium

514 Azide in 1XHBSS) for 15 minutes at room temperature and then spinned at 500g for 2 minutes  
515 to remove buffer. Primary anti-influenza A virus nucleoprotein antibodies were purchased from  
516 Millipore (MAB8258B | clone A3, biotin-conjugated). The primary antibodies were diluted  
517 1:2000 in permeable buffer and 50 µl diluted antibodies were added into each well of 96-well  
518 plate. Primary antibodies were incubated with infected cells at room temperature for 1 hour. The  
519 cells were then washed 3 times with permeable buffer. FITC conjugated goat anti-mouse  
520 secondary antibodies were purchased from Invitrogen and diluted at 1:1000 in permeable buffer.  
521 Secondary antibodies were incubated for 1 hour at room temperature and washed as described  
522 before. The stained cells were finally resuspended in 70 µl P2F. The cell suspension was run on a  
523 high throughput FACS machine (MACSQuant® analyzer 10 - Miltenyi Biotec). Uninfected cells  
524 were stained the same as infected cells and were used as negative staining cell populations. Any  
525 cells/events that had fluorescence intensity higher than all the negative staining cell population  
526 were gated as virus infection positive. Data were analyzed using flowjo software (version 10).

527

## 528 **ACCESSION CODES**

529 All raw sequencing data are deposited in GEO (small RNA sequencing: GSE80169; mRNA  
530 sequencing: GSE76901; TAILseq: GSE85893). All *C. elegans* strains created in this study will be  
531 freely available on a non-collaborative basis. Correspondence and requests for materials should be  
532 addressed to E.A.M. ([eam29@cam.ac.uk](mailto:eam29@cam.ac.uk)).

533

534

535

536

537 **REFERENCES**

- 538 1. Ding, S.-W. & Voinnet, O. Antiviral immunity directed by small RNAs. *Cell* **130**, 413–  
539 426 (2007).
- 540 2. Goubau, D., Deddouche, S. & Reis e Sousa, C. Cytosolic Sensing of Viruses. *Immunity*  
541 **38**, 855–869 (2013).
- 542 3. Schoggins, J. W. *et al.* A diverse range of gene products are effectors of the type I  
543 interferon antiviral response. *Nature* **472**, 481–485 (2011).
- 544 4. Félix, M.-A. *et al.* Natural and experimental infection of *Caenorhabditis* nematodes by  
545 novel viruses related to nodaviruses. *PLoS Biol.* **9**, e1000586 (2011).
- 546 5. Ashe, A. *et al.* A deletion polymorphism in the *Caenorhabditis elegans* RIG-I homolog  
547 disables viral RNA dicing and antiviral immunity. *Elife* **2**, e00994 (2013).
- 548 6. Ashe, A., Sarkies, P., Le Pen, J., Tanguy, M. & Miska, E. A. Antiviral RNAi against  
549 Orsay virus is neither systemic nor transgenerational in *Caenorhabditis elegans*. *J. Virol.*  
550 **89**, JVI.03664–14–12046 (2015).
- 551 7. Guo, Y. R. *et al.* Crystal structure of a nematode-infecting virus. *Proc. Natl. Acad. Sci.*  
552 *U.S.A.* **111**, 12781–12786 (2014).
- 553 8. Jiang, H. *et al.* Orsay virus utilizes ribosomal frameshifting to express a novel protein that  
554 is incorporated into virions. *Virology* **450-451**, 213–221 (2014).
- 555 9. Franz, C. J. *et al.* Orsay, Santeuil and Le Blanc viruses primarily infect intestinal cells in  
556 *Caenorhabditis* nematodes. *Virology* **448**, 255–264 (2014).
- 557 10. Sarkies, P., Ashe, A., Le Pen, J., McKie, M. A. & Miska, E. A. Competition between  
558 virus-derived and endogenous small RNAs regulates gene expression in *Caenorhabditis*  
559 *elegans*. *Genome Res.* **23**, 1258–1270 (2013).



- 560 11. Guo, X., Zhang, R., Wang, J., Ding, S.-W. & Lu, R. Homologous RIG-I-like helicase  
561 proteins direct RNAi-mediated antiviral immunity in *C. elegans* by distinct mechanisms.  
562 *Proc. Natl. Acad. Sci. U.S.A.* **110**, 16085–16090 (2013).
- 563 12. Fan, Y. *et al.* Structure of a pentameric virion-associated fiber with a potential role in  
564 Orsay virus entry to host cells. *PLoS Pathog.* **13**, e1006231 (2017).
- 565 13. Duchaine, T. F. *et al.* Functional proteomics reveals the biochemical niche of *C. elegans*  
566 DCR-1 in multiple small-RNA-mediated pathways. *Cell* **124**, 343–354 (2006).
- 567 14. Tabara, H., Yigit, E., Siomi, H. & Mello, C. C. The dsRNA binding protein RDE-4  
568 interacts with RDE-1, DCR-1, and a DExH-box helicase to direct RNAi in *C. elegans*.  
569 *Cell* **109**, 861–871 (2002).
- 570 15. van Wolfswinkel, J. C. *et al.* CDE-1 affects chromosome segregation through uridylation  
571 of CSR-1-bound siRNAs. *Cell* **139**, 135–148 (2009).
- 572 16. Olsen, A., Vantipalli, M. C. & Lithgow, G. J. Checkpoint proteins control survival of the  
573 postmitotic cells in *Caenorhabditis elegans*. *Science* **312**, 1381–1385 (2006).
- 574 17. Kwak, J. E. & Wickens, M. A family of poly(U) polymerases. *RNA* **13**, 860–867 (2007).
- 575 18. Heo, I. *et al.* TUT4 in concert with Lin28 suppresses microRNA biogenesis through pre-  
576 microRNA uridylation. *Cell* **138**, 696–708 (2009).
- 577 19. Norbury, C. J. Cytoplasmic RNA: a case of the tail wagging the dog. *Nat. Rev. Mol. Cell*  
578 *Biol.* **14**, 643–653 (2013).
- 579 20. Wickens, M. & Kwak, J. E. Molecular biology. A tail tale for U. *Science* **319**, 1344–1345  
580 (2008).
- 581 21. Lee, M., Kim, B. & Kim, V. N. Emerging roles of RNA modification: m(6)A and U-tail.  
582 *Cell* **158**, 980–987 (2014).

- 583 22. Rissland, O. S. & Norbury, C. J. Decapping is preceded by 3' uridylation in a novel  
584 pathway of bulk mRNA turnover. *Nat. Struct. Mol. Biol.* **16**, 616–623 (2009).
- 585 23. Morgan, M. *et al.* mRNA 3' uridylation and poly(A) tail length sculpt the mammalian  
586 maternal transcriptome. *Nature* **548**, 347–351 (2017).
- 587 24. Lim, J. *et al.* Uridylation by TUT4 and TUT7 marks mRNA for degradation. *Cell* **159**,  
588 1365–1376 (2014).
- 589 25. Chang, H., Lim, J., Ha, M. & Kim, V. N. TAIL-seq: Genome-wide Determination of  
590 Poly(A) Tail Length and 3' End Modifications. *Mol. Cell* **53**, 1044–1052 (2014).
- 591 26. Miki, T. S., Rügger, S., Gaidatzis, D., Stadler, M. B. & Großhans, H. Engineering of a  
592 conditional allele reveals multiple roles of XRN2 in *Caenorhabditis elegans* development  
593 and substrate specificity in microRNA turnover. *Nucleic Acids Res.* **42**, 4056–4067  
594 (2014).
- 595 27. Kamath, R. S. *et al.* Systematic functional analysis of the *Caenorhabditis elegans* genome  
596 using RNAi. *Nature* **421**, 231–237 (2003).
- 597 28. Molleston, J. M. *et al.* A conserved virus-induced cytoplasmic TRAMP-like complex  
598 recruits the exosome to target viral RNA for degradation. *Genes Dev.* **30**, 1658–1670  
599 (2016).
- 600 29. Huo, Y. *et al.* Widespread 3'-end uridylation in eukaryotic RNA viruses. *Sci Rep* **6**, 25454  
601 (2016).
- 602 30. Samji, T. Influenza A: understanding the viral life cycle. *Yale J Biol Med* **82**, 153–159  
603 (2009).
- 604 31. Rehwinkel, J. Is anti-viral defence the evolutionary origin of mRNA turnover? (Comment  
605 on DOI 10.1002/bies.201600100). *Bioessays* **38**, 817–817 (2016).

- 606 32. Hamid, F. M. & Makeyev, E. V. Exaptive origins of regulated mRNA decay in  
607 eukaryotes. *Bioessays* **38**, 830–838 (2016).
- 608 33. Manokaran, G. *et al.* Dengue subgenomic RNA binds TRIM25 to inhibit interferon  
609 expression for epidemiological fitness. *Science* **350**, 217–221 (2015).

610

611

612

613

614

615

616

617

618

619

620

621

622

623

624

625

626

627

628

629 **ACKNOWLEDGMENTS**

630 We thank Mélanie Tanguy for OrV viral filtrates, Lise Frézal for help with the OrV RNA FISH,  
631 Isabel Wilkinson for support with the genetic screen, Nicolas J. Lehrbach for help with  
632 microinjections, and Marc Ridyard for lab management. We thank Kay Harnish, Fabian  
633 Braukmann and Sylviane Moss for high-throughput sequencing support. We are grateful to V.  
634 Narry Kim and Hyeshik Chang for sharing information on TAIL-seq and Adrianus C.M. Boon for  
635 providing IAV. We thank the International *C. elegans* gene knockout consortium and the  
636 TransgeneOme project for providing reagents. We thank Vladimir Benes and the EMBL genome  
637 core for sequencing support. We thank George Allen and Charles Bradshaw for core  
638 bioinformatics support. We thank Ragini Medhi and Dick Zijlmans for help with TUTs Western  
639 blots. This work was supported by Cancer Research UK (C13474/A18583, C6946/A14492), the  
640 Wellcome Trust (104640/Z/14/Z, 092096/Z/10/Z) and The European Research Council (ERC,  
641 grant 260688). DW holds an Investigator in the Pathogenesis of Infectious Disease Award from  
642 the Burroughs Wellcome Fund.

643

644 **AUTHOR INFORMATION**

645 The authors have made the following declarations about their contributions: Conceived and  
646 designed the experiments: J.L.P., H.J., E.A.M. Performed the experiments: J.L.P., H.J., E.K., J.K.,  
647 C.L., M.M., C.M. Analyzed the data: J.L.P., H.J., T.D.D., K.L.M.R., A.J.E, D.O.C., D.W., EAM.  
648 Wrote the manuscript: J.L.P., E.A.M.

649

650

651

## 652 TABLES

653 Table 1 | Ovid screen candidate genes

Genotype	High viral load?	RNAi intact?	High sdz-6 level?	Candidate gene	Candidate variation	Brief description
WT	No	Yes	Yes			
<i>rde-1</i>	Yes	No	Yes			RNAi factor
<i>drh-1</i>	Yes	Yes	No			Viral RNA receptor
<i>ovid-1</i>	Yes	Yes	No	<i>drh-1</i>	Glu834Lys	Viral RNA receptor
<i>ovid-2</i>	Yes	Yes	Yes	n.d.		
<i>ovid-3</i>	Yes	No	Yes	<i>mut-16</i>	Gln861*	RNAi factor
<i>ovid-4</i>	Yes	No	Yes	<i>rde-4</i>	Ala220Thr	RNAi factor
<i>ovid-5</i>	Yes	No	Yes	n.d.		
<i>ovid-6</i>	Yes	Yes	Yes	T09B4.2	Pro330Leu	Putative rho guanine nucleotide exchange factor
<i>ovid-7</i>	Yes	Yes	Yes	C41D11.6	Gly596Ser	Putative RNA nuclease
<i>ovid-8</i>	Yes	Yes	Yes	n.d.		
<i>ovid-9</i>	Yes	Yes	Yes	<i>cde-1</i>	Gln910*	Terminal uridylyltransferase
<i>ovid-10</i>	Yes	No	Yes	<i>rrf-1</i>	Gly45Glu	RNAi factor
<i>ovid-11</i>	Yes	Yes	Yes	C54D10.14	Gly122Arg	Uncharacterized, DRH-1-dependent induction
<i>ovid-12</i>	Yes	No	Yes	F27D4.6	Arg717*	Uncharacterized
<i>ovid-13</i>	n.s.	Yes	Yes	n.d.		
<i>ovid-14</i>	n.s.	Yes	Yes	n.d.		
<i>ovid-15</i>	n.s.	Yes	Yes	n.d.		
<i>ovid-16</i>	Yes	Yes	Yes	<i>phi-32</i> <i>ssl-1</i>	Pro75Ser Gly1119Glu	Ubiquitin gene SNF2-related

654 n.s., not scored. n.d., not determined.

655

656 **FIGURES**

657 **Figure 1 | A forward genetic screen identifies novel antiviral immunity genes**

658 **a**, Diagram of the *lys-3p::gfp* viral stress sensor.

659 **b**, Ovid screen workflow. Transgenic animals carrying the viral stress sensor were mutagenized  
660 using EMS and F2 progeny were assayed. OrV, Orsay virus. Ovid, Orsay virus immunodeficient.

661 **c**, Top panel: viral load of strains as indicated, measured by qRT-PCR of OrV RNA1, 4 dpi. Error  
662 bars represent the standard error of the mean (SEM) of four biological replicates. One-tailed  
663 student's t-test: \*\*\*\*p<0.0001, \*\*\* p<0.001, \*\*p<0.01, \*p<0.05. Bottom panel: locomotion  
664 defects scored (paralyzed or twitching) after *unc-22* RNAi feeding. Error bars: SEM, three  
665 biological replicates. Two-tailed student's t-test: \*\*\*\*p<0.0001, \*\*p<0.01.

666 **d**, Viral load compared to *sdz-6* mRNA levels by qRT-PCR. Error bars: SEM of four biological  
667 replicates. Samples as in **c**.

668

669 **Figure 2 | The terminal uridylyltransferase CDE-1 restricts viral infection**

670 **a**, Diagram of *cde-1* alleles. DAD, catalytic dead mutant.

671 **b**, Neighbor joining tree of the terminal uridylyl transferases (TUTs) of *C. elegans* and humans  
672 and *S. pombe* CID1.

673 **c**, Diagrams of *C. elegans* CDE-1 and human TUT4 and TUT7. Domains were predicted by  
674 Interpro. The central D of the conserved DDD catalytic triad is highlighted in red.

675 **d**, Viral load as measured by qRT-PCR of OrV RNA1 genome in adults two days after infection.  
676 Five biological replicates per sample. One-tailed student's t-test: \*\*\*\* p<0.0001, \*\*p<0.01

677

678

679 **Figure 3 | CDE-1 acts in parallel to antiviral RNAi**

680 **a**, Schematic of antiviral RNAi in *C. elegans*. Viral Recognition Complex (ViRC) includes DCR-  
681 1; DRH-1; RDE-4.

682 **b**, Comparison between the viral load and primary viRNA populations. Primary viRNAs (23-  
683 nucleotide long, from 5' monophosphate RNA sequencing). Only antisense RNAs were considered  
684 to exclude potential viral genome degradation products. Each data point represents one biological  
685 replicate (population of animals).

686 **c**, Comparison between the viral load and secondary viRNA populations. Secondary viRNAs (22-  
687 nucleotide long, starting with a G, from 5' tri/monophosphate RNA sequencing). Samples as in **b**.

688 **d and e**, Viral load as measured by qRT-PCR of OrV RNA1 genome in adults two days after  
689 infection. Five biological replicates per sample. One-tailed student's t-test: \*\*\*  $p < 0.001$ ,  
690 \*\* $p < 0.01$ , \* $p < 0.05$ . Samples as in **b**.

691

692 **Figure 4 | CDE-1 directly targets the Orsay virus RNA genome for uridylation**

693 **a**, Schematic of TUT-mediated RNA degradation.

694 **b**, Poly(A) tail length distribution measured by TAIL-seq after two days of OrV infection. Vertical  
695 grey line represents the mean of *cde-1* and wild type peaks (38 nt).

696 **c**, Schematic of Orsay virus replication

697 **d**, Most frequent collapsed reads after RACE-seq on OrV RNA1 and RNA2 (2 dpi), respectively.  
698 Non-templated residues (absent from the reference genome) are indicated in red.

699 **e**, Percentage reads with non-templated nucleotides detected at the 3' end of OrV RNA1-2 in strains  
700 as indicated, two days post infection. Two biological replicates per genotype.

701 **f**, Percentage reads with a non-templated mono-uridyl residue at the 3' end of OrV RNA2, upon  
702 RNAi-mediated gene knockdown as indicated, one day post infection. Two biological replicates  
703 per sample.

704

705 **Figure 5 | Antiviral RNAi and virus terminal uridylation are parallel immune defense**  
706 **pathways in *C. elegans*.** Virion cartoon adapted from <sup>12</sup>.

707

708 **Figure 6 | The terminal uridylyltransferases TUT4/7 attenuate Influenza A mRNAs in**  
709 **mammalian cells**

710 **a**, Schematic of Influenza A virus replication

711 **b-d**, Most frequent collapsed reads after RACE-seq on IAV NP cRNA, NP vRNA and NP  
712 mRNA, respectively in A549 cells at 8 hpi.

713 **e**, Percentage of reads with a non-templated U-tail (no U-tail; 1 U; 2 Us or  $\geq 3$  Us) in different  
714 RNAs as indicated measured by RACE-seq in A549 cells 8 hpi.

715 **f**, Percentage of reads with a non-templated U-tail (as in **e**) in MEF cells of different genotypes  
716 as indicated (with two independently created cell lines per genotype).

717 **g-h**, Percentage of infected cells measured by immunofluorescence against NP (FACS). Error:  
718 SEM, three biological replicates. MEFs *Tut4/7* KO are full null independent lines.

719

720

721

722

723



724 **EXTENDED DATA FIGURES**

725 **Extended Data Figure 1 | The viral stress sensor (*lys-3p::GFP*) is constitutively active in some**  
726 **tissues but is induced in the intestine upon severe viral infection.**

727 **a**, Comparison of viral load and the *lys-3* and *sdz-6* mRNA expression after two days of infection  
728 by qRT-PCR, strains as indicated. Each data point represents one biological replicate (population  
729 of animals on one agar plate). Samples as in Fig. 3d,e.

730 **b**, Representative confocal sections (10× or 20× magnification, as specified) of the viral stress  
731 sensor in wild type and *drh-1* mutants without infection. The viral stress sensor exhibited  
732 constitutive activity in uninfected individuals, which was restricted to specific tissues. GFP was  
733 observed at all developmental stages in the pharynx and the rectum of hermaphrodites.  
734 Additionally, hermaphrodites at the L4 larval stage would show a strong GFP signal around the  
735 vulva and gravid adults exhibited the GFP in the uterine lumen. In males, GFP was observed in  
736 the pharynx and the tail. GFP expression was comparable in wild type and *drh-1* mutants and  
737 independent of viral infection. Thus, the gene *lys-3* is constitutively active in tissues neighboring  
738 openings exposed to the environment, the most likely entry points of potential bacterial pathogens.

739 **c**, Representative confocal sections (20× magnification) of young adults (strains as indicated)  
740 carrying the viral stress sensor. Animals were uninfected (mock) or infected with OrV for four  
741 days. The viral stress sensor was strongly induced in the intestine after infection of *drh-1* mutants,  
742 which is in agreement with the tropism of OrV. Intestinal GFP was most often visible around the  
743 collar of the nematodes, in the anterior region of the intestine in young adults. Some infected  
744 individuals exhibited a strong GFP signal throughout their entire body (data not shown),  
745 suggesting that the induction of the viral stress sensor can spread from cell to cell, like an

746 inflammation process. The viral stress sensor offers an opportunity to easily monitor viral  
747 infections in living animals.

748

749 **Extended Data Figure 2 | A *cde-1* deletion allele fails to complement the screen isolate *ovid-***  
750 **9.**

751 **a**, Workflow of *cde-1/ovid-9* (*mj414*) × *cde-1* (*tm1021*) F8 recombinant family generation. A  
752 similar strategy was used to construct the *cde-1* (*mj414*) × *drh-1* (*ok3495*) F8 recombinant families.  
753 All animals were homozygous for the viral stress sensor (*mjIs228*).

754 **b-c**, Number of families that activated the viral stress sensor in more than 20% of individuals after  
755 four days of infection with OrV. Approximately 50 individuals were scored per agar plate.

756

757 **Extended Data Figure 3 | *cde-1* mutants show horizontal transmission of Orsay virus**  
758 **infection**

759 Workflow and data monitoring the inter-individual transmission of OrV infection (in strains as  
760 indicated) using the viral stress sensor.

761

762 **Extended Data Figure 4 | Intestinal expression of *cde-1* confers antiviral immunity**

763 **a**, Representative confocal sections (20× magnification) of OrV *in vivo* RNA FISH.

764 **b**, Representative confocal section (10× magnification) of a *C. elegans* L4 larva expressing *cde-*  
765 *1::GFP*. As two previous reports disagreed about the expression pattern of CDE-1<sup>15,16</sup>, we used  
766 fosmid-recombineering to generate transgenic animals driving GFP expression from an  
767 endogenous genomic context.

768 **c**, Diagram of the *cde-1* rescue transgene, using the intestine-specific promoter of the gene *vha-6*.  
769 This transgene was injected in *cde-1* null mutants.

770 **d**, Viral load as measured by qRT-PCR of OrV RNA1 genome in adults two days after infection.  
771 Error: SEM, five biological replicates. One-tailed student's t-test: \*\*\*  $p < 0.001$ , \*\* $p < 0.01$ .

772 **e**, Incidence of male in the progeny of hermaphrodites left to self-fertilize at 25°C, in strains as  
773 indicated.

774

#### 775 **Extended Data Figure 5 | CDE-1 is not required for general miRNA homeostasis**

776 **a**, Non-templated nucleotides at the 3' end of the different classes of endogenous and antiviral  
777 small RNAs as indicated. RNA was isolated from young adults after two days of infection with  
778 OrV.

779 **b**, miRNA expression in *cde-1 (tm1021)* mutants as compared to wild type, samples as in **a**.

780 **c**, piRNAs and endogenous 22G-RNAs abundance in *cde-1 (tm1021)* mutants as compared to wild  
781 type, normalised to library size. Each data point represents one biological replicate. Samples as in  
782 **a**.

783

#### 784 **Extended Data Figure 6 | CDE-1-depleted animals show a high expression of stress response** 785 **genes during Orsay virus infection**

786 **a**, Fold change in the length of poly(A) tails (measured by TAIL-seq) in *cde-1* mutants compared  
787 to wild type. RNA was isolated from young adults after two days of OrV infection.

788 **b**, Differential mRNA expression in *cde-1 (tm1021)* compared to wild type, two days of OrV  
789 infection (mRNA-seq).

790

791 **Extended Data Figure 7 | The 3' end of the Orsay virus genome contains CDE-1-dependent**  
792 **non-templated U-tails**

793 **a**, Simplified workflow of 3' RACE-seq of OrV RNA1 and OrV RNA2.

794 **b-c**, Comparison between the viral load and the fraction of non-templated mono(U) tails at the 3'  
795 end of OrV RNA1 and OrV RNA2, respectively, in strains as indicated. Each data point represents  
796 one biological replicate. Samples as in Fig. 3d,e and Fig. 4e.

797

798 **Extended Data Figure 8 | The terminal uridylyltransferases TUT4/7 restrict Influenza A infection**

799 **a**, Protein level of the IAV NP measured by immunofluorescence (FACS). Error: SEM in three  
800 biological replicates.

801 **b**, Level of expression of the IAV NP mRNA normalized to *Gapdh* in MEF cells of different  
802 genotypes as indicated. Error: SEM, three biological replicates.

803

804

805

806

807

808

809

810

811

812 **SUPPLEMENTARY INFORMATION**

813 **Supplementary Table 1 | Infection by the Orsay virus induces viral stress sensor in Ovid**  
 814 **screen isolates.**

Strain	Genotype	% intestinal GFP mock	% intestinal GFP OrV
SX2635	WT	0	4
SX2615	<i>rde-1</i>	0	42
SX2790	<i>drh-1</i>	0	83
SX2996	<i>ovid-1</i>	0	86
SX2900	<i>ovid-2</i>	0	83
SX2739	<i>ovid-3</i>	0	74
SX2901	<i>ovid-4</i>	0	73
SX2902	<i>ovid-5</i>	0	68
SX2729	<i>ovid-6</i>	0	64
SX2991	<i>ovid-7</i>	0	60
SX2990	<i>ovid-8</i>	0	52
SX3000	<i>ovid-9</i>	0	48
SX2881	<i>ovid-10</i>	0	47
SX2987	<i>ovid-11</i>	0	46
SX2988	<i>ovid-12</i>	0	44
SX2920	<i>ovid-13</i>	0	26
SX2909	<i>ovid-14</i>	0	26
SX2886	<i>ovid-15</i>	0	24
SX2885	<i>ovid-16</i>	0	24

815  
 816 The percentage of young adults exhibiting intestinal GFP was assessed after four days of  
 817 infection by OrV or in non-infected animals (mock). 20 to 50 young adults were scored per plate,  
 818 in three biological replicates (average values are shown here). The screen isolates *ovid-*  
 819 *1,7,8,9,11,12* were backcrossed prior to GFP scoring (see Supplementary Table 2).

820  
 821  
 822  
 823  
 824  
 825

Supplementary Table 2 | *C. elegans* strains used in this study

Genotype	Strain	Comment
+	N2	
<i>cde-1(mj453)</i> III	SX3186	
<i>cde-1(tm1021)</i> III	RF1290	
<i>cde-1(tm1021)</i> III ; <i>drh-1(ok3495)</i>	SX2998	
IV		
<i>cde-1(tm1021)</i> III ; <i>mjEx595</i>	SX3265	Contains the intestine-specific <i>cde-1</i> construct ( <i>vha-6p::cde-1</i> )
<i>cde-1(tm1021)</i> III ; <i>mjIs228</i> ?	SX2999	
<i>cde-1(tm1021)</i> III ; <i>rde-1(ne219)</i> V	SX3004	
<i>drh-1(ok3495)</i> IV	RB2519	
<i>drh-1(ok3495)</i> IV ; <i>mjIs228</i> ?	SX2790	
F27D4.6( <i>tm1098</i> )	FX01098	
I		
<i>mjEx594</i> ?	SX3123	Contains the <i>cde-1::GFP</i> fosmid (TransgeneOme construct)
<i>mjIs228</i> ?	SX2635	Contains the biostress ( <i>lys-3p::GFP</i> ) reporter
<i>ovid-1(mj417)</i>	SX2996	Backcrossed 2X to SX2635
<i>ovid-2(mj422)</i>	SX2900	
<i>ovid-3(mj367)</i>	SX2739	
<i>ovid-4(mj423)</i>	SX2901	
<i>ovid-5(mj425)</i>	SX2902	
<i>ovid-6(mj357)</i>	SX2729	
<i>ovid-7(mj405)</i>	SX2991	Backcrossed 2X to SX2635
<i>ovid-8(mj369)</i>	SX2990	Backcrossed 2X to SX2635
<i>ovid-9(mj414)</i>	SX3000	Backcrossed 2X to SX2635
<i>ovid-10(mj403)</i>	SX2881	
<i>ovid-11(mj354)</i>	SX2987	Backcrossed 3X to SX2635
<i>ovid-12(mj401)</i>	SX2988	Backcrossed 3X to SX2635
<i>ovid-13(mj432)</i>	SX2920	
<i>ovid-14(mj431)</i>	SX2909	
<i>ovid-15(mj408)</i>	SX2886	
<i>ovid-16(mj407)</i>	SX2885	
<i>rde-1(ne219)</i> V	WM27	
<i>rde-1(ne219)</i> V ; <i>mjIs228</i> ?	SX2615	

828 **Supplementary Table 3 | Primers used in this study**

Name	Sequence	Description
M1835	TGGAGCCGACTATGTTCGTTGAG	RT-qPCR on <i>gapdh</i> - left
M1836	GCAGATGGAGCAGAGATGATG AC	RT-qPCR on <i>gapdh</i> - right
M4410	ACCTCACAACCTGCCATCTACA	RT-qPCR OrV RNA1 - left
M4411	GACGCTTCCAAGATTGGTATT	RT-qPCR OrV RNA1 - right
M4988	CAATGCATTTGAAGCTGGAC	RT-qPCR on <i>lys-3</i> - left
M4989	CCATTAGCAAGCAAATTCTGG	RT-qPCR on <i>lys-3</i> - right
M5041	ACAATCGGGCGTTCAATTC	RT-qPCR on <i>sdz-6</i> - left
M5042	TCTGATAGCTGGCTGAGTGG	RT-qPCR on <i>sdz-6</i> - right
M5472	GGGGACAACCTTTGTATAGAAAA GTTGCTTCGAAAGAAACCCAAT CCTC	cloning of <i>lys-3p</i> into gateway system - left
M5473	GGGGACTGCTTTTTTTGTACAAA CTTGGAGGAGCTGGGAAAGAG TAGCA	cloning of <i>lys-3p</i> into gateway system - right
M7316	CCGGAACCCATCACGAAATT	PCR on <i>cde-1 (mj414)</i> for Sanger sequencing - left
M7317	TCCATTTCAAAGTCTCCACAGA	PCR on <i>cde-1 (mj414)</i> for Sanger sequencing - right
M7454	ATGGCCAAACGTCTGAAACC	OrV RNA1 3' RACE - left
M7455	CCAAAGTCGCTTGCTGTACA	OrV RNA2 3' RACE - left
M7456	CCTTGGCACCCGAGAATTCCA	OrV RNA1/2 3' RACE - right
M7601	G TTCAGAGTTCTACAGTCCGAC GATCATGGCCAAACGTCTGAAA CC	OrV RNA1 3' RACE (with TruSeq RA5 sequence) - left
M7602	G TTCAGAGTTCTACAGTCCGAC GATCCCAAAGTCGCTTGCTGTA CA	OrV RNA2 3' RACE (with TruSeq RA5 sequence) - left
M8443	GCTAATTGGGCAAGGAGACG	IAV 3' RACE PB2 RNA complementary left
M8444	GCTGGGTTCTTCTCCTGTCT	IAV 3' RACE PB2 RNA genomic left
M8451	CTCTCGGACGAAAAGGCAAC	IAV 3' RACE NP RNA complementary left
M8452	AAGTTCGGTGCACATTTGGA	IAV 3' RACE NP RNA genomic left
M8453	CGCAATCTGGACTAGTGGGA	IAV 3' RACE NA RNA complementary left
M8454	GCCTTGGTTGCATATTCCAGT	IAV 3' RACE NA RNA genomic left

M8455	ACGGTTTGAAAAGAGGGCCT	IAV 3' RACE MP RNA complementary left
M8456	CGGTGTTCTTCCCTGCAAAG	IAV 3' RACE MP RNA genomic left
M8459	G TTCAGAGTTCTACAGTCCGAC GATCgctaattgggcaaggagacg	IAV 3' RACE PB2 RNA complementary left (with TruSeq RA5 sequence)
M8460	G TTCAGAGTTCTACAGTCCGAC GATCgctgggttctctctgtct	IAV 3' RACE PB2 RNA genomic left (with TruSeq RA5 sequence)
M8467	G TTCAGAGTTCTACAGTCCGAC GATCctctcggacaaaaggcaac	IAV 3' RACE NP RNA complementary left (with TruSeq RA5 sequence)
M8468	G TTCAGAGTTCTACAGTCCGAC GATCaagtcggtgcacatttggga	IAV 3' RACE NP RNA genomic left (with TruSeq RA5 sequence)
M8469	G TTCAGAGTTCTACAGTCCGAC GATCcgcaatctggactagtggga	IAV 3' RACE NA RNA complementary left (with TruSeq RA5 sequence)
M8470	G TTCAGAGTTCTACAGTCCGAC GATCgccttggtgcatattccagt	IAV 3' RACE NA RNA genomic left (with TruSeq RA5 sequence)
M8471	G TTCAGAGTTCTACAGTCCGAC GATCacggtttgaaaagagggcct	IAV 3' RACE MP RNA complementary left (with TruSeq RA5 sequence)
M8472	G TTCAGAGTTCTACAGTCCGAC GATCcggtgttctcctgcaaag	IAV 3' RACE MP RNA genomic left (with TruSeq RA5 sequence)
M8652	CCTTCCACAATGCCAAAGTT	gapdh gene specific RT primer
M8581	CCAGATCGTTCGAGTCGTTTTTT TTTTTTTTTTCTTTAATTGTC	IAV NP mRNA gene specific RT primer
M8651	GGGTGTGAACCACGAGAAAT	gapdh qRT-PCR primer left
M8652	CCTTCCACAATGCCAAAGTT	gapdh qRT-PCR primer right
M8582	CCAGATCGTTCGAGTCGT	IAV NP mRNA qRT-PCR primer left
M8583	CGATCGTGCCCTCCTTTGCGAT CGTGCCCTCCTTTG	IAV NP mRNA qRT-PCR primer right
HJ359	GATGGACAAACAGACAAACC	Tut4-1GTF genotyping
HJ360	GCAGTTGTGCTATATTGACTC	Tut4-1GTR genotyping
HJ365	TGATCAGAGCATGCATACTC	Tut7-2GTF genotyping
HJ366	AAACAAGAAGCAGAGGTCCA	Tut7-2GTR genotyping

829

830

831

832



833 **ADDITIONAL REFERENCES**

- 834 34. Brenner, S. The genetics of *Caenorhabditis elegans*. *Genetics* **77**, 71–94 (1974).  
835 35. Fire, A. Integrative transformation of *Caenorhabditis elegans*. *EMBO J.* **5**, 2673–2680  
836 (1986).  
837 36. Jorgensen, E. M. & Mango, S. E. The art and design of genetic screens: *caenorhabditis*  
838 *elegans*. *Nat. Rev. Genet.* **3**, 356–369 (2002).  
839 37. Sarov, M. *et al.* A genome-scale resource for in vivo tag-based protein function  
840 exploration in *C. elegans*. *Cell* **150**, 855–866 (2012).  
841 38. Dobin, A. *et al.* STAR: ultrafast universal RNA-seq aligner. *Bioinformatics* **29**, 15–21  
842 (2013).  
843 39. Liao, Y., Smyth, G. K. & Shi, W. featureCounts: an efficient general purpose program for  
844 assigning sequence reads to genomic features. *Bioinformatics* **30**, 923–930 (2014).  
845 40. Love, M. I., Huber, W. & Anders, S. Moderated estimation of fold change and dispersion  
846 for RNA-seq data with DESeq2. *Genome Biol.* **15**, 550 (2014).  
847 41. Paix, A., Folkmann, A., Rasoloson, D. & Seydoux, G. High Efficiency, Homology-  
848 Directed Genome Editing in *Caenorhabditis elegans* Using CRISPR-Cas9  
849 Ribonucleoprotein Complexes. *Genetics* **201**, 47–54 (2015).  
850 42. Martin, M. Cutadapt removes adapter sequences from high-throughput sequencing reads.  
851 *EMBnet.journal* **17**, 10 (2011).  
852 43. Harris, T. W. *et al.* WormBase 2014: new views of curated biology. *Nucleic Acids Res.*  
853 **42**, D789–93 (2014).  
854 44. Quinlan, A. R. & Hall, I. M. BEDTools: a flexible suite of utilities for comparing genomic  
855 features. *Bioinformatics* **26**, 841–842 (2010).  
856 45. Robinson, M. D., McCarthy, D. J. & Smyth, G. K. edgeR: a Bioconductor package for  
857 differential expression analysis of digital gene expression data. *Bioinformatics* **26**, 139–  
858 140 (2010).  
859 46. Zhang, J., Kobert, K., Flouri, T. & Stamatakis, A. PEAR: a fast and accurate Illumina  
860 Paired-End reAd mergeR. *Bioinformatics* **30**, 614–620 (2014).  
861 47. Kawakami, E. *et al.* Strand-specific real-time RT-PCR for distinguishing influenza vRNA,  
862 cRNA, and mRNA. *J. Virol. Methods* **173**, 1–6 (2011).  
863

Figure 1. Le Pen et al.

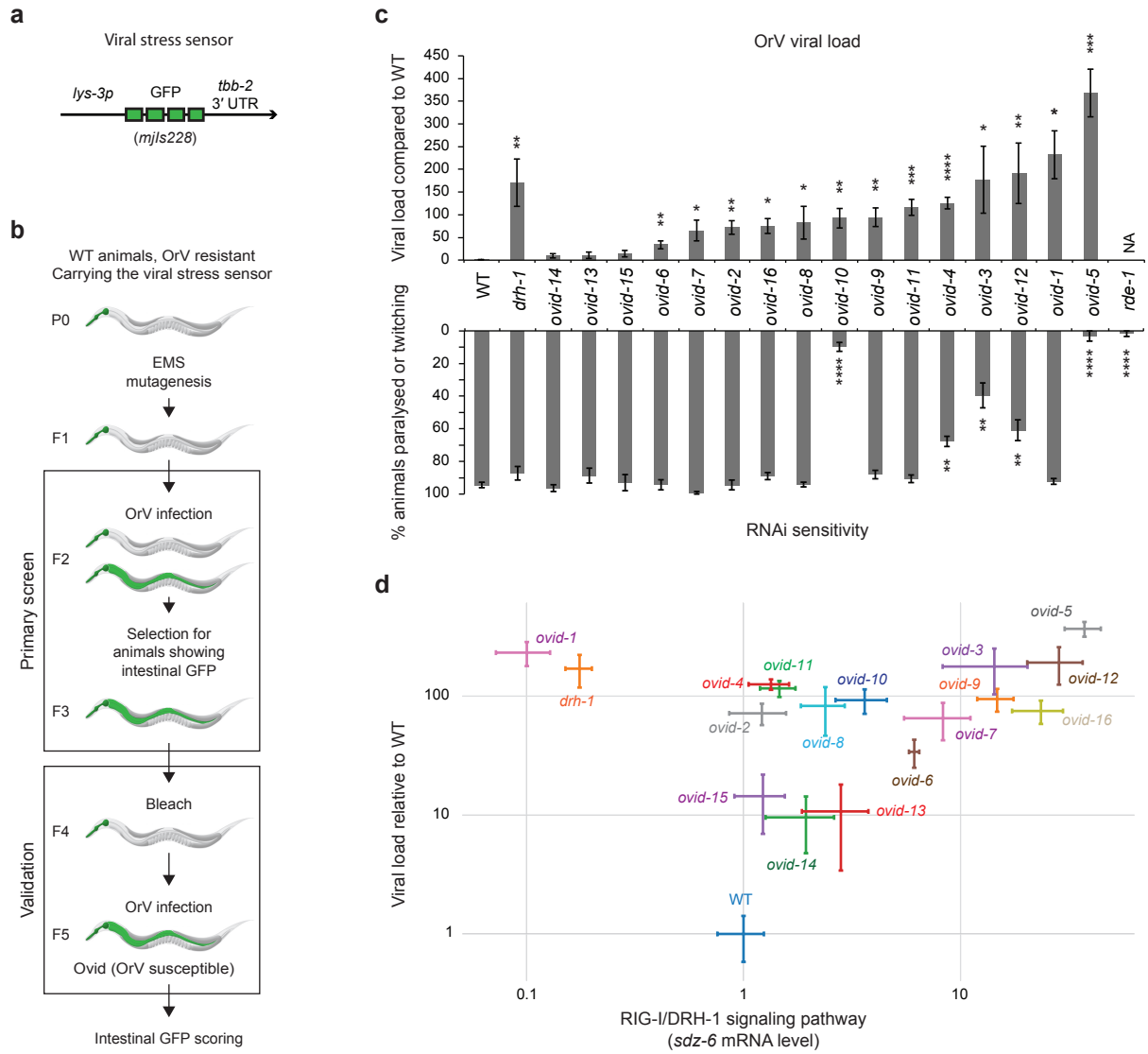


Figure 2. Le Pen et al.

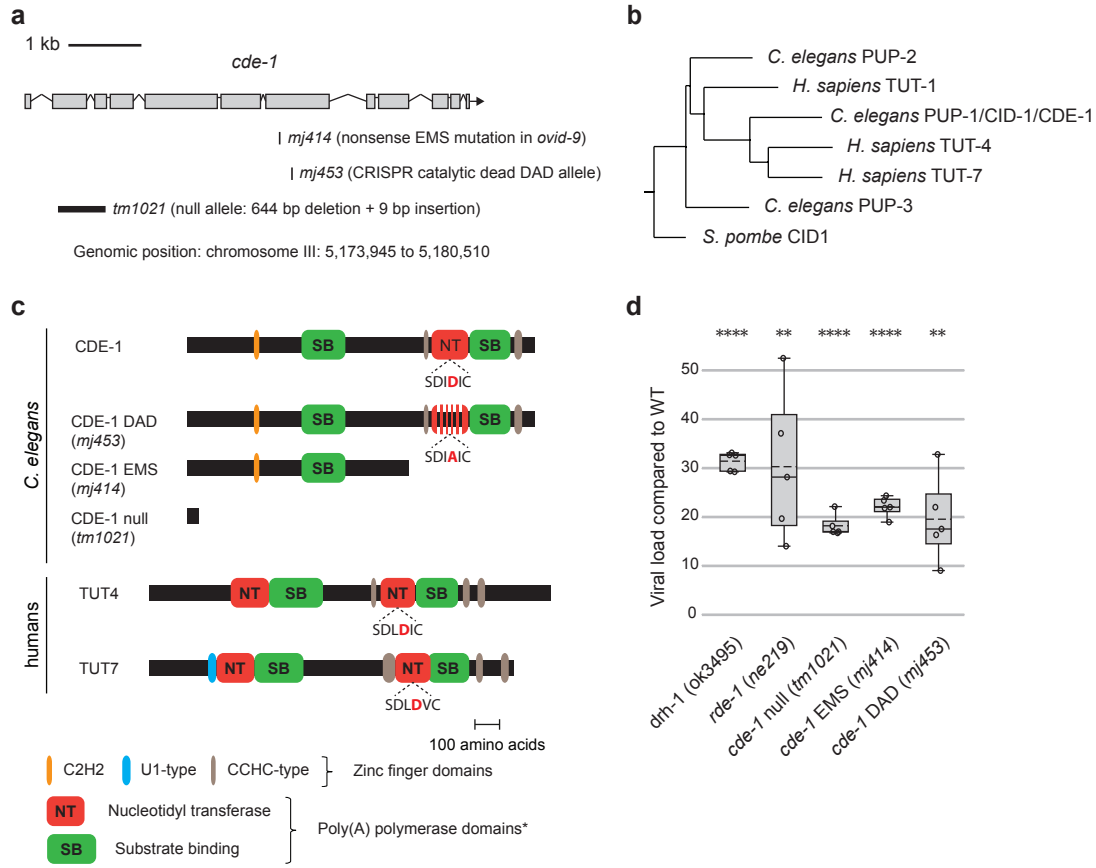


Figure 3. Le Pen et al.

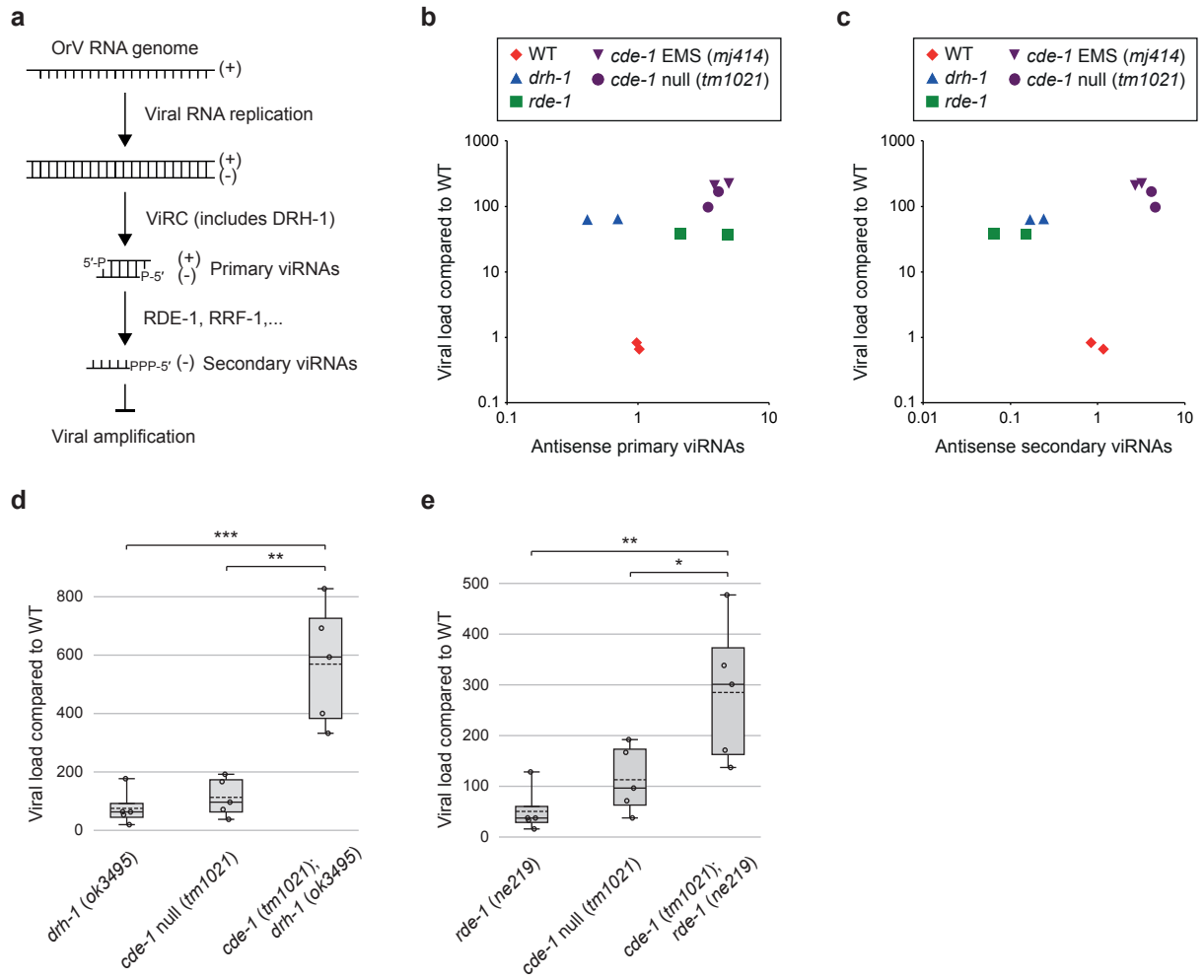


Figure 4. Le Pen et al.

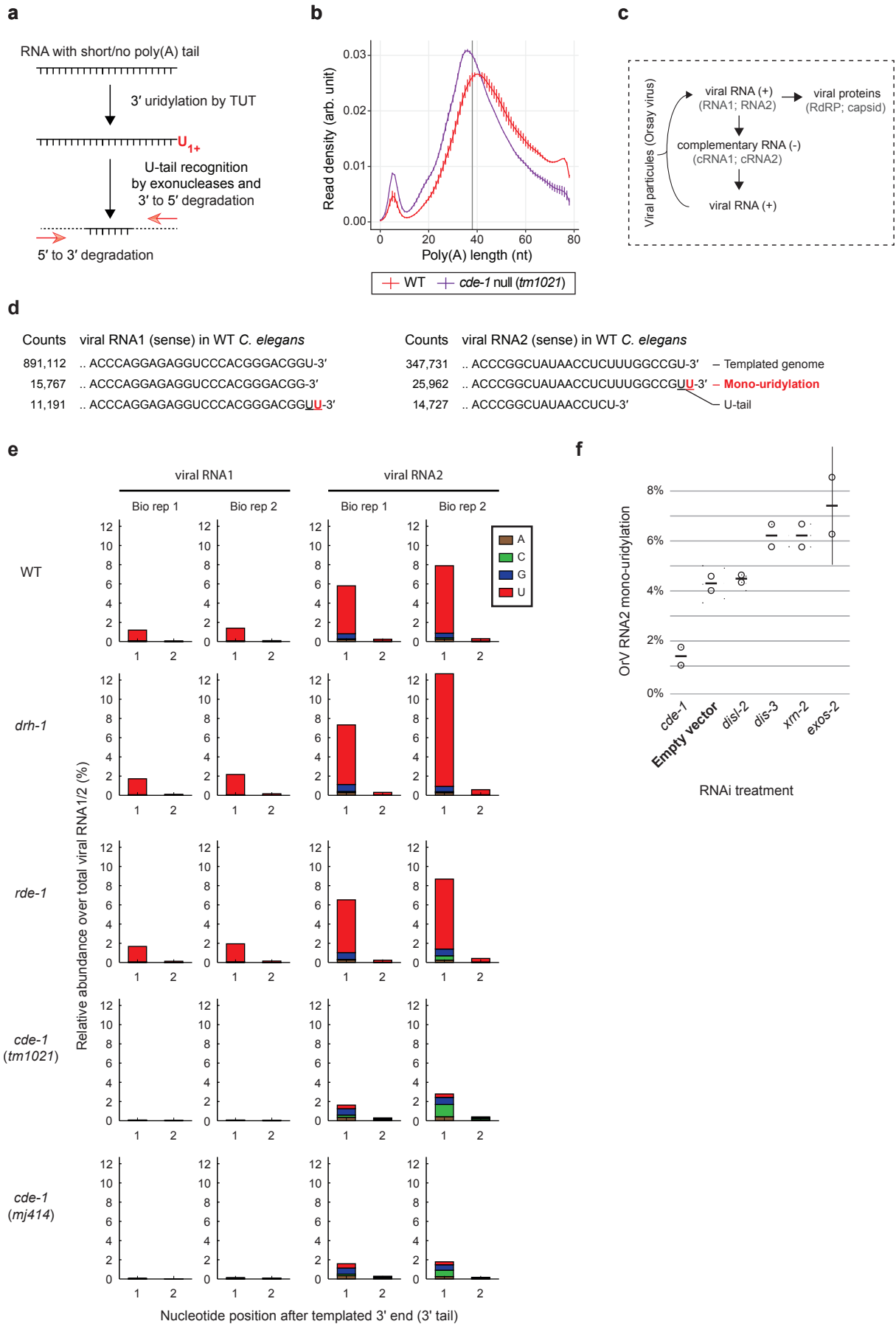


Figure 5. Le Pen et al.

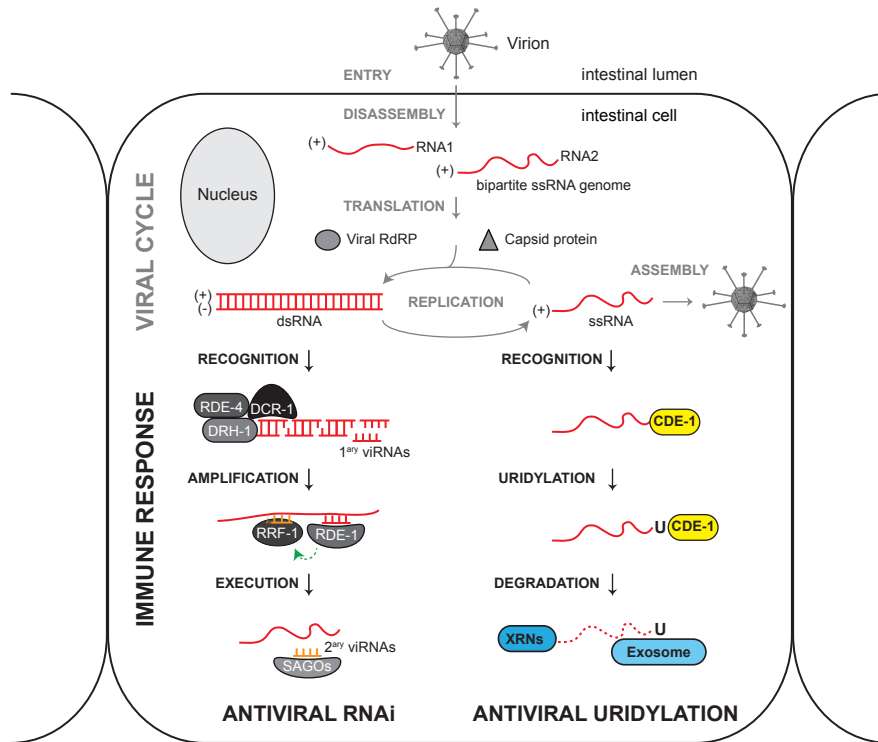
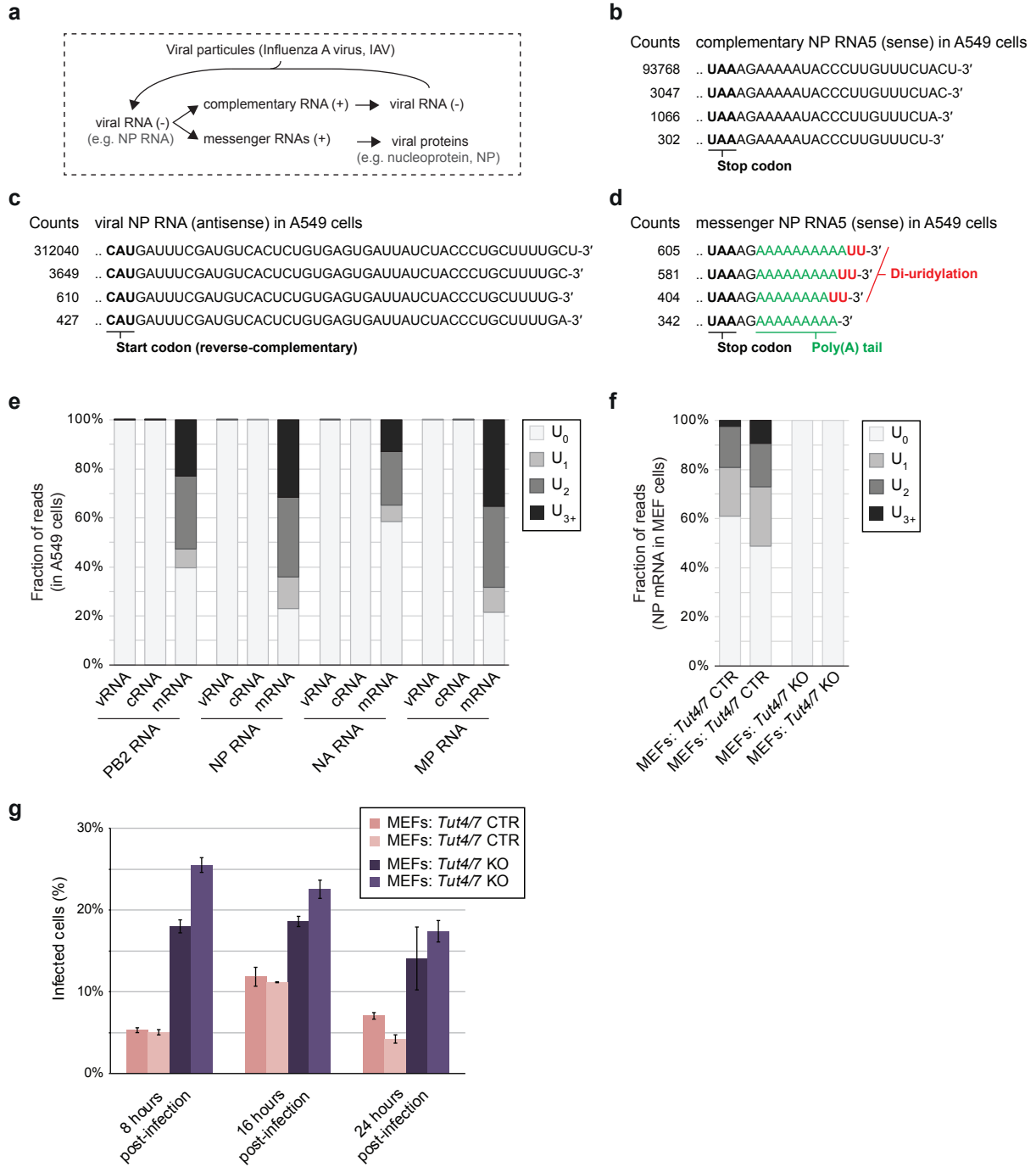
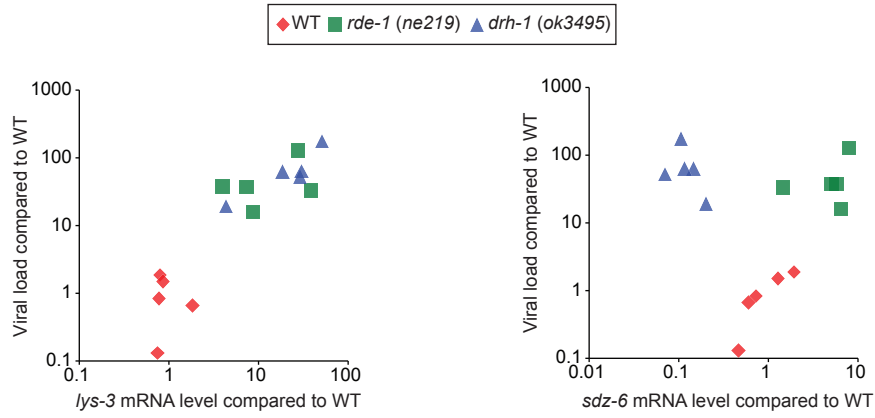


Figure 6. Le Pen et al.

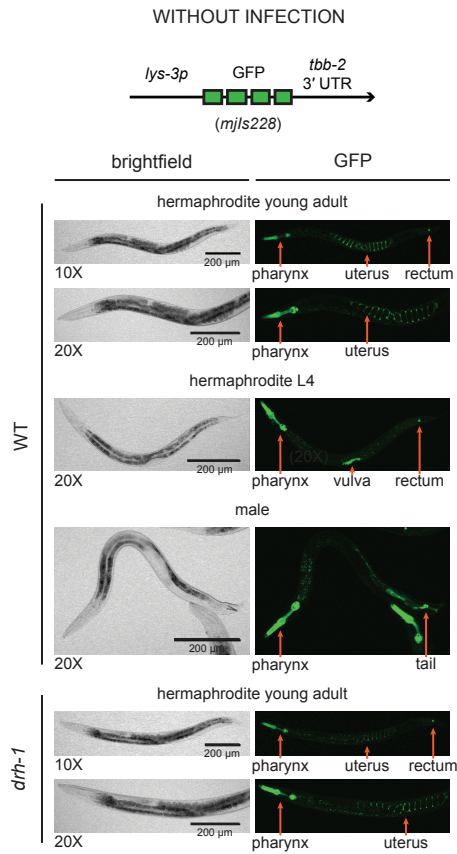


Extended data figure 1. Le Pen et al.

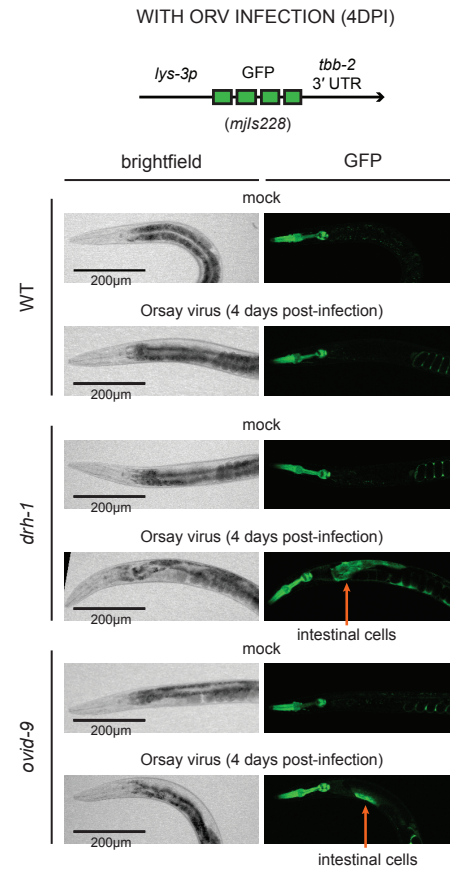
**a**



**b**



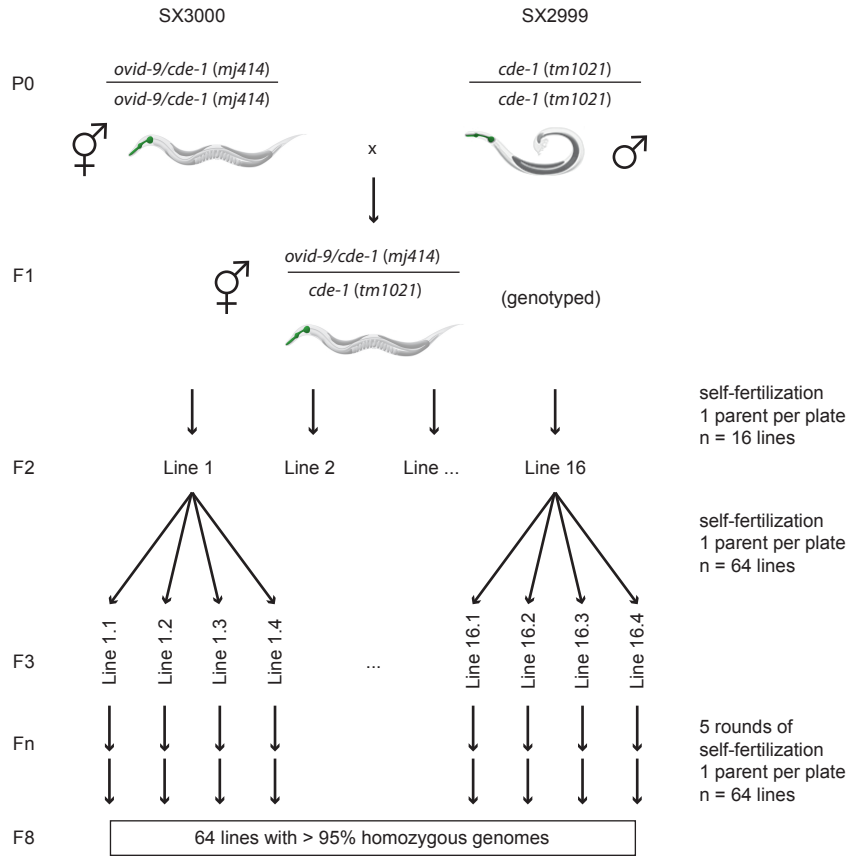
**c**



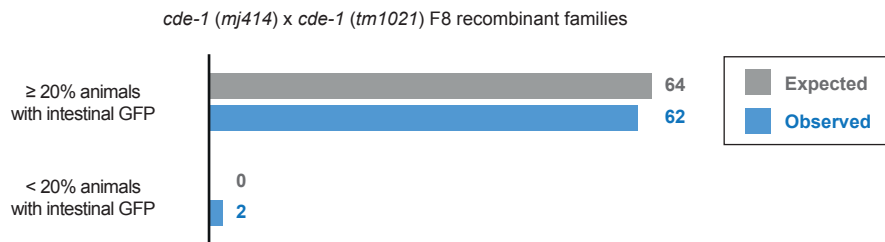


Extended data figure 2. Le Pen et al.

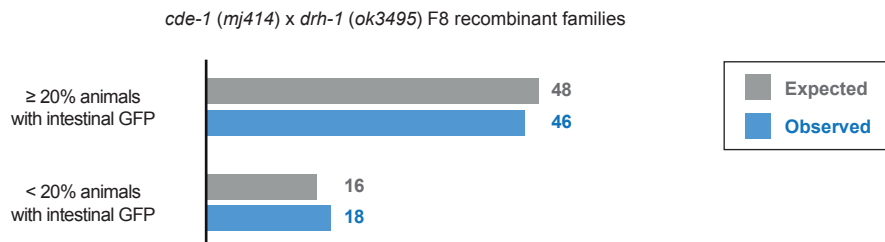
**a**



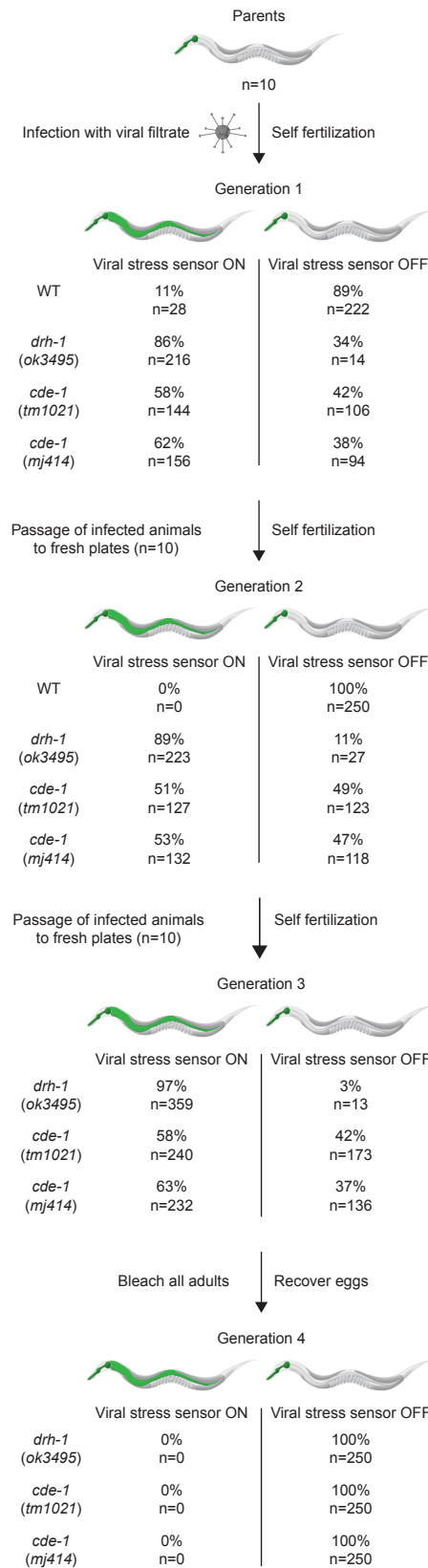
**b**



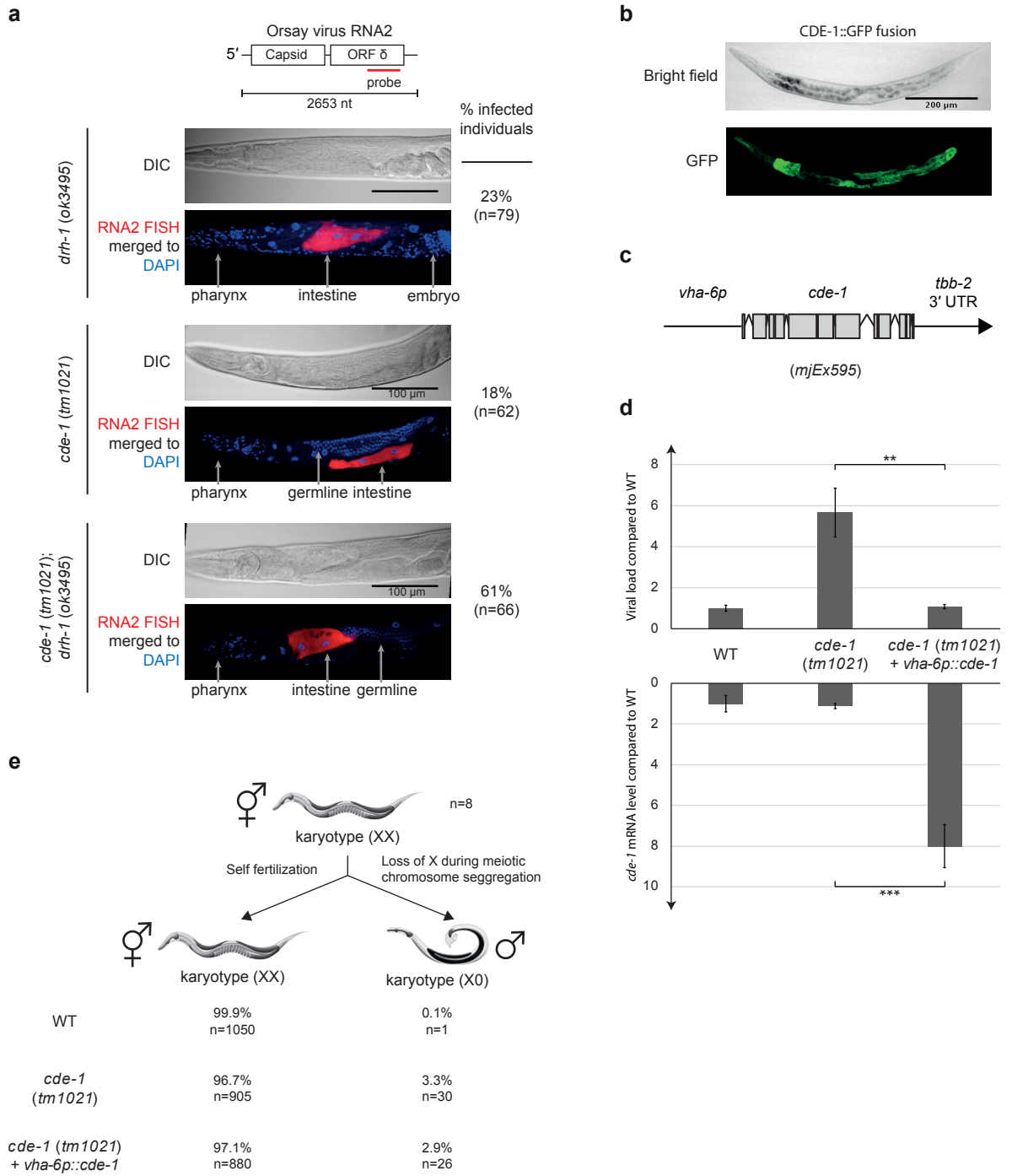
**c**



# Extended data figure 3. Le Pen et al.

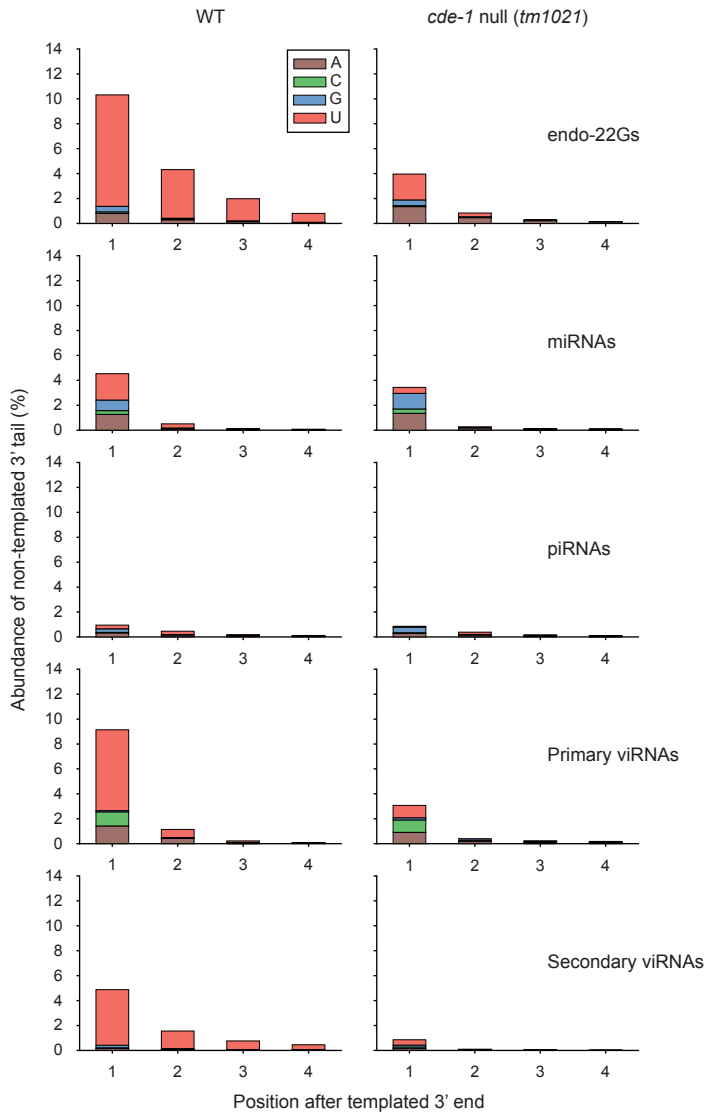


Extended data figure 4. Le Pen et al.

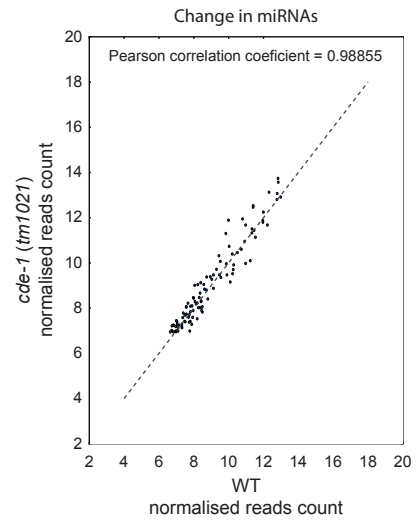


Extended data figure 5. Le Pen et al.

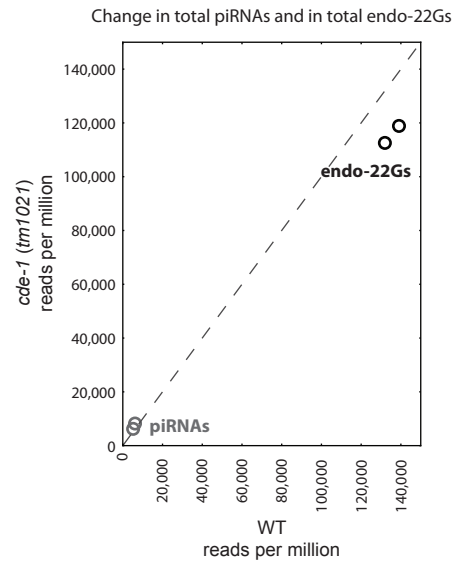
**a**



**b**

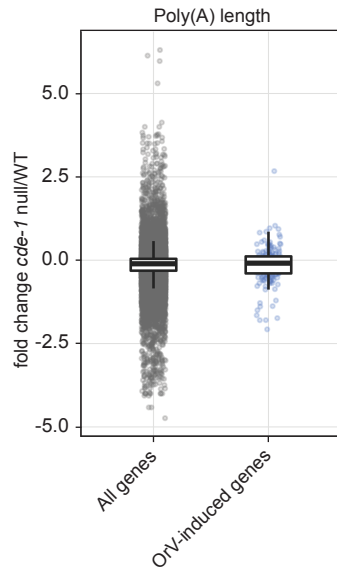


**c**

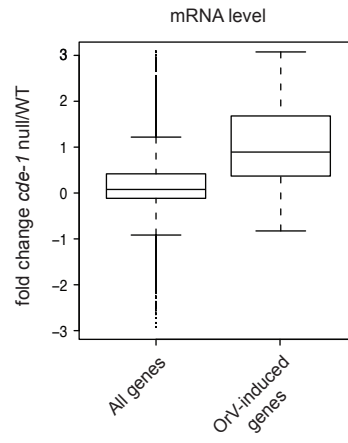


Extended data figure 6. Le Pen et al.

**a**

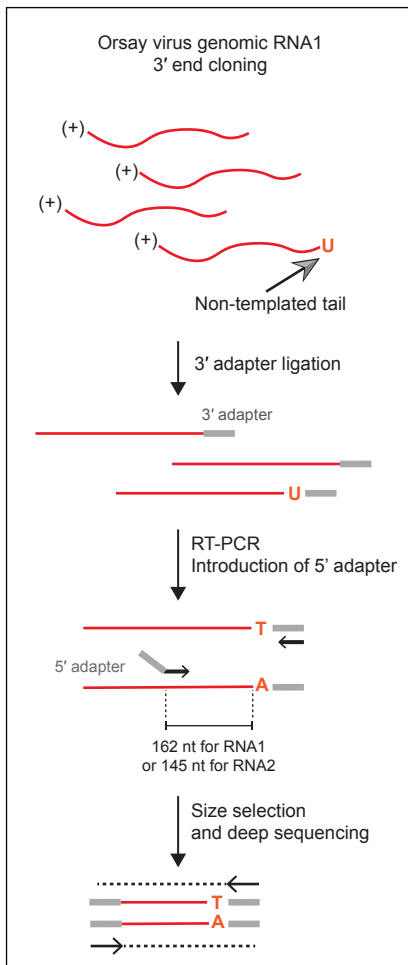


**b**

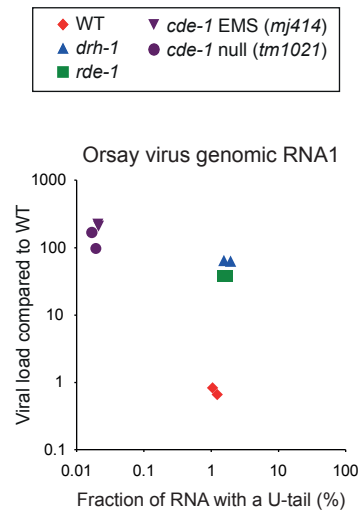


Extended data figure 7. Le Pen et al.

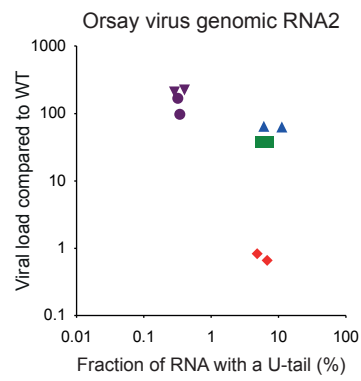
**a**



**b**

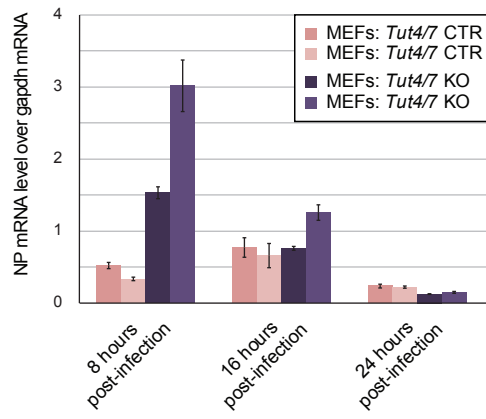


**c**



Extended data figure 8. Le Pen et al.

**a**



**b**

